MATHEMATIC MODELLING OF KINETICS FOR THE CRYSTALLIZATION OF TUNGSTIC ACID FROM ELECTROLYTICALLY TREATED SODIUM TUNGSTATE SOLUTION

Arnoldus Johannes Fourie.

A dissertation submitted to the Faculty of Engineering, University of the Witwatersrand, Johannesburg, in fulfilment of the requirements for the degree of Master of Science in Engineering.

Johannesburg, 1987

DECLARATION

I declare that this dissertation is my own, unaided work. It is being submitted for the Degree of Master of Science in Engineering in the University of the Witwatersrand, Johannesburg. It has not been submitted for any degree or examination in any other University.

4th day of June 1987.

ABSTRACT

The nucleation and growth rate kinetics for the continuous crystallization of tungstic acid from solution was studied in a 0.8 l evaporative mixed suspension, mixed product removal crystallizer. The crystallizer included a draft tube which improved the uniformity of the suspension. Experimental conditions which were varied during the experimental runs were drawdown time of the crystallizer, stirrer speed of the stirrer in solution, heat flux to the crystallizing solution and the suspension density of the crystallizing magma.

X-ray diffraction patterns of the tungstic acid material produced confirmed that the material was crystalline and that it was in the tungsten monohydrate ($WO_3.H_2O$) form.

The crystal size distribution of the crystallizer magma was obtained under steady state conditions and used to calculate the crystal nucleation and growth rates. The main nucleation mechanism in the crystallizing system was contact secondary nucleation and the crystal growth rates were found to be crystal size dependent. A size dependant growth rate model was proposed which was incorporated in the population balance equation. Good fits of the model to the data were obtained using this population balance equation.

Analysis of the expressions derived for the nucleation and nuclei sized crystal growth rates indicated that the nucleation rate was a linear function of crystallizer magma suspension density and that there existed an inverse relationship between the nucleation rate and the crystal growth rate of the nuclei sized crystals.

Hierdie MSc dra ek met graagte op aan my ouers vir al hulle liefde en ondersteuning in hierdie tyd.

ACKNOWLEDGEMENTS

I would like to thank the following people and institutions:

Dr. B. Verbaan for his advice and guidance in his capacity as supervisor for this dissertation.

Mr. D.F. Williams and Dr. K. Brooks for the use of their word processing program.

Dr. D. Boydell for his valuable support and for arranging the particle size analysis of the crystal samples at the Council for Mineral Technology (MINTEK).

MINTEK, for financing the project.

The University of the Witwatersrand for the extensive use of their facilities.

Boart Hard Metals (Pty) Ltd. for supplying the ammonium paratungstate samples with which the experiments were conducted.

CONTENTS

LIST OF FIGURES

LIST OF TABLES

NOMENCLATURE

Symbol	Description	Units
A_L	Specific surface area of the distribution, eq. 3.15	m^2/l
a	Distance between growth units in the crystal lattice, eq. 3.24	m
B	Empirical birth function, eq. 3.2	number/slm
B^*	Crystal nucleation rate, eq. 3.6	number/ls
c_L	Solution equilibrium concentration for crystal size L, eq. 3.21	g/l
c^*	Solution equilibrium concentration, eq. 3.21	g/l
D	Empirical death function, eq. 3.2	number/slm
d	Interplanar distance in a crystal, eq. 3.4	m
F	Faraday's constant, eq. C.1	C/mol
G	Crystal growth rate, eq. 3.3	m/s
G^*	Growth rate of the nuclei sized crystals, eq. 3.25	m/s
ΔG^*	Free energy of formation of a nucleus, eq. 4.1	J
h(L)	Size dependent withdrawal rate, eq. 3.17	-
I	Current density, eq. C.1	A/m^2
k	Boltzmann constant, eq. 4.1	J/K
k_a	Area shape factor, eq. 3.15	-
k_v	Volume shape factor, eq. 3.16	-
L	Characteristic crystal size, eq. 3.3	m
L_t	Sum of the characteristic lengths of all the crystals in the distribution, eq. 3.14	m
M	Molecular weight of the crystals, eq. 3.21	g/mol
M_T	Suspension density of the crystal magma, eq. 3.16	g/l
N	Molar flux, eq. D.2	mol/sm^2
N_t	Total number of crystals in a unit volume of the system, eq. 3.11	number/l
N(L)	Cumulative number of particles in a population distribution, eq. 3.1	number/l
n(L)	Population density distribution function, eq. 3.2	number/lm
n^*	Population density of the nuclei sized crystals, eq. 3.5	number/lm
p	Number of parameters in the model, eq. 6.4	-

Q_j	The j th input or output volumetric flowrate to the volume V, eq. 3.2	l/s
R	Gas constant, eq. 3.21	J/Kmol
S	Supersaturation of the crystallizing solution, eq. 3.23	g/l
S_R	Least sum of squares, eq. 6.4	
s	Measure of the roughness of the crystal surface, eq. 3.24	-
T	Absolute temperature, eq. 3.21	K
t	Time	s
V	Total volume of the crystallizing suspension, eq. 3.2	l
v_i	Internal particle velocity of the crystal, eq. 3.2	m/s
ΔW	Weight fraction of crystals in a specific size range, section 6.3	-

Greek Symbols

τ	Drawdown time of the crystallizer vessel, eq. 3.4	s
ρ	Crystal mass density, eq. 3.16	g/l
γ	Surface energy, eq. 3.21	J/m^2
λ	Wave length, eq. 5.4	m
λ_s	Mean displacement of the crystal surface, eq. 3.24	m
σ	Surface tension, eq. 4.2	g/s^2
θ	Angle of incidence or reflection of the X-ray beam, eq. 5.4	-
η	Membrane efficiency, eq. C.1	-

1. INTRODUCTION

Most modern commercial tungsten plants use either a chloride-based process or a soda ash pressure leaching operation for the recovery of ammonium paratungstate (APT) from scheelite concentrates. Various problems exist in these processes such as corrosion and high maintenance costs for the chloride-based process and effluent disposal problems for the soda ash pressure leaching operation.

In order to try and eliminate these various problems Verbaan (1985) proposed a flowsheet which utilises the soda ash pressure leaching step in conjunction with two electrolytic membrane processes. These electrolytic membrane processes are used to eliminate some of the effluent disposal problems encountered in the soda ash operation and permit possible recovery of reagents, as well as allow the production of APT via a tungstic acid intermediate.

The production of this tungstic acid intermediate is done using an evaporative crystallization technique. This technique has various possible advantages such as additional purification possibilities and the ability to closely control the crystal size distribution (CSD) of the tungstic acid crystals. Direct calcination of the crystals to the tungsten oxide or tungsten powder products thus eliminating the APT intermediate, is also a possibility.

Such a tungstic acid crystallization step promises to be commercially very attractive if fully exploited, and therefore the main part of this dissertation will be concerned with the modelling of tungstic acid crystallization kinetics.

The remaining portion of chapter 1 gives some background on the different processes which are or can be used to extract tungsten metal from basic ores. This is done to highlight the significance of the

1. INTRODUCTION

Most modern commercial tungsten plants use either a chloride-based process or a soda ash pressure leaching operation for the recovery of ammonium paratungstate (APT) from scheelite concentrates. Various problems exist in these processes such as corrosion and high maintenance costs for the chloride-based process and effluent disposal problems for the soda ash pressure leaching operation.

In order to try and eliminate these various problems Verbaan (1985) proposed a flowsheet which utilises the soda ash pressure leaching step in conjunction with two electrolytic membrane processes. These electrolytic membrane processes are used to eliminate some of the effluent disposal problems encountered in the soda ash operation and permit possible recovery of reagents, as well as allow the production of APT via a tungstic acid intermediate.

The production of this tungstic acid intermediate is done using an evaporative crystallization technique. This technique has various possible advantages such as additional purification possibilities and the ability to closely control the crystal size distribution (CSD) of the tungstic acid crystals. Direct calcination of the crystals to the tungsten oxide or tungsten powder products thus eliminating the APT intermediate, is also a possibility.

Such a tungstic acid crystallization step promises to be commercially very attractive if fully exploited, and therefore the main part of this dissertation will be concerned with the modelling of tungstic acid crystallization kinetics.

The remaining portion of chapter 1 gives some background on the different processes which are or can be used to extract tungsten metal from basic ores. This is done to highlight the significance of the

proposed flowsheet and the importance of the crystallization process. Section 1.1 discusses the basic uses of tungsten and gives a broad overview of what the basic steps are for the recovery of the tungsten metal. Section 1.2 describes the two existing tungsten recovery processes currently in operation in more detail. In section 1.3 is a complete description of the new process proposed by Verbaan (1985). Finally, the scope and objective of this study are defined in section 1.4.

1.1 Extractive metallurgy of tungsten

Tungsten is the eighteenth most abundant metal, having an estimated concentration in the earth's crust of 1 ppm. During the nineteenth century tungsten remained a laboratory material. The latter half of the century saw the development of high speed tool steels containing tungsten which became the prime use for the metal in the first half of the twentieth century. Today, the manufacture of cemented carbides accounts for over half of the tungsten consumption in the world (Stephen and Wang, 1981).

According to Stephen and Wang (1981) the term "extractive metallurgy" refers to those process steps that start with an ore concentrate and end with an intermediate compound that can be reduced to yield metallic tungsten of desired purity and metallurgical properties. The objective of the extractive process is thus to convert the tungsten value contained in the ore concentrate to the intermediate compound, usually synthetic scheelite, tungstic acid or ammonium paratungstate (APT). Generally, the ore concentrate is given a pretreatment to remove impurities that may be difficult or more expensive to eliminate at a later stage. The next step is the ore decomposition, in which the tungsten is isolated from other major constituents of the ore and converted to a form in which subsequent purification is feasible. Some purification is also accomplished during ore decomposition. Finally, the remaining impurities are removed, and the desired intermediate compound (APT, or H_2WO_4) is obtained. It is very

important that a high purity tungsten compound is obtained since high purity is required for all uses of tungsten except as a steel-alloying additive.

1.2 Processes for the production of tungsten

The two main processes described below to produce tungsten from scheelite ($CaWO_4$) are via a chloride-based process or via a soda ash pressure leaching operation.

1.2.1 The chloride-based process

Ore decomposition using HCl leaching is often the process selected when high-purity natural or synthetic scheelite minerals are available and the molybdenum level in the final product is not critical.

According to Stephen and Wang (1981), the first step is the decomposition of the high-grade scheelite with hydrochloric acid:

$$CaWO_4 + 2HCl \rightleftharpoons CaCl_2 + H_2WO_4 \qquad 1.1$$

Since $CaCl_2$ is soluble in aqueous hydrochloric acid, the precipitated tungstic acid can be isolated by filtration and washing. The equilibrium constant, $K=[CaCl_2]/[HCl]^2$ is large (i.e. $K=10^4$) and the reaction should go to completion with the stoichiometric amount of acid. However, in practice large excess amounts of HCl are required to complete the reaction. This is because of the slow diffusion of HCl through the layer of H_2WO_4 that forms around the $CaWO_4$ particles. In order to increase the leaching rate, high HCl concentrations, excess amounts of the acid, high temperatures, effective agitation, and small particle sizes of the ore concentrates are employed (Stephen

and Wang, 1981).

According to Canterford and Colton (1968) some separation of molybdenum from tungsten occurs during the acid leach. This results from the grossly differing solubilities of molybdic and tungstic acids in HCl. The extend of molybdenum removed depends on the amount and concentration of HCl used and the efficiency of filtration and washing.

Filtration of tungstic acid slurry is of special importance in impurity removal and in material recovery. Stephen and Wang (1981) suggest that when iron is present as an impurity, use of small amounts of nitrate or other oxidation reagents during digestion is recommended: This will oxidize the ferrous ions to ferric ions which precipitate and facilitate filtration.

The further preparation of pure APT from crude tungstic acid involves three steps: Digestion of the tungstic acid in aqueous ammonia, filtration of the ammonium tungstate solution, and crystallization of the APT.

In aqueous ammonia, removal of phosphorus and arsenic may be accomplished by the addition of a little magnesium oxide, which forms insoluble magnesium ammonium phosphate and arsenate under these conditions. Iron and similar metals form colloidal hydroxides and their removal together with silica, which is also colloidal, is accomplished by the addition of a small amount of activated carbon and by digesting for 1-2 hrs. Filtration is rather slow but can be efficiently accomplished by the use of a pressure filter with filter aids (Stephen and Wang, 1981).

APT crystals are obtained by evaporating the purified ammonium tungstate solution, and the amount of crystals formed depends upon the

extend of evaporation. Partial impurity removal is accomplished during the crystallization process. Removal of molybdenum is especially noticeable.

The APT crystals are then calcined to tungsten oxide and further reduced to tungsten metal powder.

Some of the disadvantages of this chloride-based process are:

a)Large excess amounts of HCl are used for the leaching of the scheelite ore. This large excess amount of acid must be neutralised using limestone. The resulting neutral dissolved salt, calcium chloride, represents a pollutant. Environmental legislations for the disposal of aqueous effluents are stringent and the cheap disposal of affluents containing significant concentrations of such dissolved salts is generally not possible. The excess acid cannot be recovered.

b)The water associated with substantial concentrations of dissolved salts cannot be recycled and needs to be disposed of. This represents another cost, and a waste of water.

c)In any process where chlorides are present corrosion is a problem and increases maintenance costs.

d)This process can only be used to process high grade scheelite ores.

1.2.2 The soda ash pressure leaching process

Low-grade ores can be decomposed ing this process. This process uses a sodium carbonate solution to decompose scheelite. The process as described by Stephen and Wang (1981) is as follows:

$$Na_2CO_3 + CaWO_4 \rightarrow Na_2WO_4 + CaCO_3 \qquad 1.2$$

As practised in industry, the leaching process is run with -44 to -90 μm concentrates at 190-225 °C for 1.5-4 hrs using 10-18 % sodium carbonate solution with 250-450 % of the stoichiometric quantity of Na_2CO_3, depending on the grade of concentrate used. The temperature employed results in pressuras of 12-26 bars, and the reaction is thus carried out in mild steel or alloy steel autoclaves.

The process is simple and effective; its advantages are that high- or low-grade concentrates of either scheelite or low-manganese wolframite may be used, and that the maintenance costs are relatively low. A frequent criticism of the process is that a large amount in excess of sodium carbonate is necessary to obtain an acceptable recovery.

The extend to which impurities present in the concentrate are rendered soluble by the leaching process is important. Experiments have shown that arsenic and phosphorous are less completely leached than tungsten, so the ratios of As/W and P/W are reduced, sometimes as much as tenfold. However, they are usually present in the leach liquor in sufficient quantity that subsequent purification is necessary. Tin remains virtually unattacked by the autoclave-soda process. When silica occurs in the leach liquor special methods must be used for its removal.

Filtration of the leach liquor to remove the gangue material is

relatively easy with both scheelite and wolframite concentrates.

The resulting sodium tungstate solution generated using this process still contains some of the impurities present in the raw material. These must be reduced to acceptable levels before the intermediate compound is prepared. The most frequently encountered contaminants are silica, phosphorous, arsenic, and molybdenum. The removal of these impurities will be discussed in Appendix A since it is a general method used in various processes for purification purposes.

After purification the sodium tungstate solution is now stripped from the alkali metals using a liquid solvent extraction process. This process extracts the tungsten from the sodium tungstate solution, leaving sodium in the aquaous phase. This sodium will be converted to sodium sulphate. The tungsten is subsequently stripped from the solvent using aqueous ammonia, and the intermediate product, APT, is obtained by crystallization from the mother liquor as described before. It must be noted that impurities such as molybdenum, silicon, phosphorous, and arsenic are also extracted using the solvent extraction process, so the preceding purification steps are needed before solvent extraction can be done.

The pure APT crystals are again calcined and reduced to tungsten metal powder.

Some of the disadvantages of the soda ash pressure leaching process are:

a) Very large excess amounts of soda ash is used for the leaching step. The sulphuric acid required to effectively neutralize the excess sodium carbonate can represent a substantial cost. Such bases are also not recovered or reused. Also, the environmentally acceptable disposal of large volumes of dissolved sodium sulphate

represents a major problem.

b)During the solvent extraction process the sodium associated with the tungstate anion is converted to sodium sulphate. The original source of these sodium ions in the process can also represent a substantial cost, and this base is also not recovered or reused.

c)The water associated with substantial concentrations of dissolved salts cannot be recycled, and needs to be disposed of. Thus, another disposal cost and a waste of water.

d)Extensive purification steps have to be employed to get rid of impurities such as As, Mo, Si, and P before the liquid solvent extraction process.

1.3 Description of the process proposed by Verbaan

As mentioned before, Verbaan and Brown (1986) proposed a new flowsheet which incorporates electrolytic membrane technology and results in the production of highly supersaturated tungstic acid solutions which may be crystallized to form crystalline tungstic acid. This novel process has not yet been fully demonstrated or commercially proven.

In this flowsheet presented as fig 1.1 the soda ash pressure leaching process described in section 1.2.2 is used to the point where the sodium tungstate solution has been purified, that is, before the solvent extraction process is employed. Instead of using the solvent extraction process to produce APT two electrolytic membrane processes are employed. A full description of the relevent chemistry in the two electrolytic processes is presented in Appendix D.

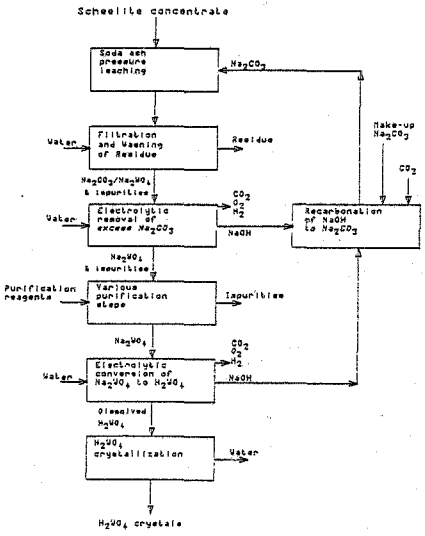

Figure 1.1 Flowsheet of the new tungsten process proposed by Verbaan

The first electrolytic membrane cell is used to remove all the excess sodium carbonate which is added in the pressure leaching step. In this process the alkali metal ions are transported across a cation selective membrane from an anode compartment to a cathode compartment. Caustic soda is formed in the cathode compartment while CO_2 and oxygen are released from the anode. The caustic soda can then be recarbonated with CO_2 to form soda ash. The soda ash now formed can then be recycled back to the pressure leaching step. This first electrolytic membrane process will be controlled in such a way that only the excess sodium carbonate is removed.

In the second electrolytic membrane process the sodium tungstate in the solution is converted to tungstic acid. Once again the alkali metal ions are transported across the membrane from the anode to the cathode. Caustic is formed in the cathode and tungstic acid is formed in the anode compartment. The caustic soda is once again recarbonated and the soda ash is recycled to the leaching step.

The pure tungstic acid solution in the anode compartment has a very high supersaturation concentration and is fed into an evaporative mixed suspension mixed product removal (MSMPR) crystallizer. Tungstic acid crystals are formed and these crystals can either be directly calcined and reduced to form tungsten metal powder, or the crystals can be redissolved in an aqueous ammonia solution and converted to the usual APT crystals. The purity of the tungstic acid crystals will determine which of the two above possible routes will be accepted. Alternatively, if the supersaturated tungstic acid solution is pure enough it can be converted directly to ammonium tungstate by the addition of ammonia, and then crystallized to form APT. It is clear that the direct calcination of the tungstic acid crystals could be the more economical route because it eludes the use of additional ammonia solutions.

From the above discussion, it follows that the two electrochemical processes represent an alternative to the solvent extraction method

discussed in section 1.2.2 for ultimately converting sodium tungstate to the tungsten oxide intermediate with the advantage that the alkaline reagent may be recovered.

Verbaan's process has the following potential advantages over the previous two processes described in section 1.2.1 and 1.2.2:

a)Virtually all of the soda ash that is used in the pressure leaching step can be recovered and recycled back to the leaching step. Thus, no acid is required for the neutralization of the soda ash and no dissolved salts require disposal of. Considerable savings arising from the recovery of soda ash and elimination of the need to use sulphuric acid can be made.

b)There are no chlorides used in this process with the result that corrosion is less.

c)Both high- and low grade scheelite as well as wolframite ores can be decomposed in this process.

d)The sodium associated with the tungstate anion is converted in the membrane cell to caustic soda which in turn can be recarbonated and recycled back to the pressure leaching step.

e)If the tungstic acid crystals can be directly calcinated and reduced to tungsten powder, no ammonium solutions are needed which also represents a saving in costs.

Disadvantages of this process are that the same purification steps used in the soda ash pressure leaching process must be applied in this process and the fact that this process has not yet been adequately demonstrated and commercially proven.

1.4 Purpose and scope of this study

The various discussions preceding this section have shown that the introduction of a new process to produce metallic tungsten will have many advantages which will favour the economics of this industry. Virtually all the steps in this new process have either been used in industry or have undergone extensive experimental research (Verbaan, Greenslade and Wade, 1984). The one aspect of this process that lacks knowledge is the kinetics associated with the crystallization of the tungstic acid from the supersaturated solution since this has never been attempted before. With this in mind the aims of this dissertation are:

a) To experimentally prove that crystalline tungstic acid can be produced from a supersaturated tungstic acid solution produced in an electrolytic membrane cell.

b) Study the nucleation and crystal growth kinetics associated with the crystallization of tungstic acid.

In order to do these investigations the following procedure was followed:

a) Pure APT crystals produced at Boart Hardmetals (Pty) Ltd. was dissolved in a stoichiometric excess amount of pure, hot caustic soda solution. This was done to permit production of sodium tungstate solutions in a reproducible manner.

b) This solution was boiled to remove the NH_3 which formed in step a.

c) This solution was treated in an electrolytic membrane cell at a current density of 1000 Amp/m^2 and a temperature that varied between 30 and 40 °C. During this process the Na^+ ions were removed from the anode compartment, and tungstic acid in solution was produced. The final Na^+ ion concentration in the anolyte so produced was typically 1 g/l or less.

d) The tungstic acid solution was continuously pumped into a 0.8 l MSMPR crystallizer which contained a draft tube circulator. The solution in the crystallizer was kept at a boiling point of 94 °C. The range of stirrer speeds in the crystallizer varied between 2400 and 4000 rpm. The range of residence times varied between 48.6 and 500 mins.

e) Samples were periodically withdrawn from the crystallizer and the tungstic acid crystals were recovered by filtration.

f) The particle size distribution of the crystals was established, and this information was processed to establish the nucleation an crystal growth kinetics.

g) The literature was reviewed to postulate crystallization mechanisms and establish mathematical models which were developed and fitted to the experimental data.

The results obtained did not follow the idealized crystallization kinetics pattern. This suggested that the crystallizing system

differed from ideal conditions and in order to correct for this a size dependent growth rate model was derived and tested.

2. THE CRYSTALLIZATION PROCESS

The main purpose of this dissertation is to study the kinetics for the crystallization of tungstic acid from a supersaturated solution produced in an electrolytic membrane cell. In order to understand why it is important to determine these kinetics, a short summary of the basic principles of crystallization from solution, either as an industrial or experimental operation, is necessary. Such an attempt has been made in this chapter: Section 2.1 briefly discusses crystallization as a separation technique. The importance of the crystal size distribution (CSD) as a property in the crystallization process is stressed in section 2.2 while some fundamental concepts which must be taken into consideration for the design of a crystallizer are presented in section 2.3. Finally, a simplified continuous crystallizing system, the idealized mixed suspension mixed product removal (MSMPR) crystallizer is described in section 2.4.

2.1 Introduction

According to de Jong (1984) crystallization is a commonly used industrial separations and purification technique. As a process for separation, crystallization is characterized by a relatively low demand for energy. This is particularly evident for cooling-crystallization if the working temperature is not far below the ambient value. Evaporative crystallization may be of interest on the grounds of energy. In evaporative crystallization, as contrasted with distillation, reflux is not used. However, the energy consumption per kg of material crystallized can be sharply reduced by means of counter current multistages utilising energy integration. The optimum number of stages can be chosen only by considering the energy optimum and capital investment costs.

In either case, whether the crystallization operation is for separation and/or purification purposes, there is a strong interaction

and dependence between both the degree of separation and purification and the particulate nature of the solid phase produced. Fundamental research on the unit operation of crystallization has focused mainly on understanding and predicting the particulate nature of the crystalline phase, recognizing that better knowledge and control of this aspect would permit improvement of the unit operation of crystallization, both as a separation and as a purification technique.

Specifically, a general theory of CSD has been advanced and refined. Various experimental and theoretical studies of the kinetics of crystal nucleation and growth rates together with particle mixing, segregation, and classification mechanics were initiated by various researchers. These particle kinetics and mechanics, which in fact establish the resulting CSD, permit analysis, evaluation, and prediction of crystallizer performance at levels of operation ranging from bench-scale to commercial production.

The development of crystallizers has the objective of producing pure crystalline materials with the minimum combined cost for capital equipment and for operating costs.

2.2 Importance of the CSD as a property in crystallization processes

CSD is one of the most important, difficult to predict, and least understood properties of crystallization processes. CSD is an important property affecting the end uses of the crystalline product as well as interacting strongly with the crystallization process itself. Randolph and Larson (1971) state that some of the more important problems in the operation of industrial crystallizers involve crystal habit and purity, salting (fouling), capacity and scale-up, and crystallizer stability. All of these problems interact strongly with the CSD in the crystallizer, and in fact, most of these problems could be listed as subheadings under the CSD. The main

mechanism of interaction of these problems with CSD is through the level of the driving force (i.e. supersaturation) in the process.

CSD also plays a major role in the economic viability of a crystallization process: The investment costs of a process for separation by means of crystallization can be considerable because small rates of growth of the crystals can result in long residence times in the crystallizer to produce a product which is coarse enough to be easily separated from the liquid. In general, long residence times imply large and therefore costly equipment. In addition, investment in equipment for separating the crystals from the liquid is necessary. The investment for such equipment is determined by the residence time to attain a suitably low residual moisture content in the end product. This residence time is again related to the resistance of the flow of a liquid through a layer of crystals which increases by a factor of 2.7 when the porosity of the crystal bed decreases from 0.6 to 0.5. Therefore, the CSD should only be allowed to vary in a limited way (de Jong, 1984).

Finally, de Jong (1984) states that the crystal size and scatter in size of the dry crystals have an effect on the resistance of the crystals to flow from silo's and on their bulk density.

2.3 Fundamental concepts in the design of crystallizers

The design of crystallizers is based on their mode of operation. The crystallization rate depends on the concentration of the feed stream, the process conditions and the equilibrium data. It is also important to decide whether this mass of crystals is to be distributed among a few large crystals or among many small crystals. This distribution is determined by the continuous interaction between nucleation kinetics and crystal growth kinetics as well as by particle classification, attrition and breakage. As mentioned earlier, the level of supersaturation is the major driving force for nucleation and growth.

Although supersaturation in a crystallizer may be very low, it is a key function in all of crystallization processes.

Crystal nucleation and growth kinetics are the two main phenomena which influence the CSD. A third is the residence time of the crystals in the crystallizer. The crystal residence time is often by default a function of the crystal dimensions. The rate of nucleation and crystal growth, and the residence time of the crystals all depend on how the mass of crystals are circulated in a crystallizer, as characterized by the time of circulation, the velocity of liquid, and the intensity of the turbulence. These factors are accounted for in the concept of hydrodynamic behaviour. The total crystal mass per unit volume, which influences the rate of nucleation, follows from the mass balance and the solubility curve of the material being crystallized. The surface area of the crystals which is available for the reduction of the supersaturation follows from the CSD and the total crystal mass per unit volume. The abrasion of the large crystals may have a significant effect on the CSD, and hence also effect the behaviour of a particular system.

According to de Jong [ ] two groups of parameters are important for the design of crystallizers.

Group 1: Crystallization kinetics, i.e., rate of nucleation, and rate of crystal growth.

Group 2: Spatial distribution of the crystal mass, i.e., the crystal mass distribution, hydrodynamic behaviour, and residence time of the crystals in the crystallizer.

The significance of these groups are different for continuous and batch crystallizers.

The research done in this study concentrated on the use of continuous crystallizers. It is for this reason that the rest of this discussion will only be concerned with continuous crystallizers.

2.4 The continuous mixed suspension mixed product removal crystallizer

In a continuous crystallizing system both the crystallization kinetics and the spatial crystal mass distribution are important in determining the CSD. Section 2.2 explained the significant role which the CSD plays in the development of an industrial crystallizer.

Crystallization kinetics are often determined using laboratory test equipment having capacities varying between 1 and 100 l. To ease analysis, results are usually obtained in an experimental crystallizer operating under steady-state conditions. It is difficult to define and determine the spatial crystal mass distribution for a continuous crystallizer. To overcome this problem the measurements for determining the kinetics are conducted in such a way that the spatial crystal mass distribution plays no part. This is accomplished by using a continuous, constant volume, isothermal, well mixed crystallizer with mixed product removal. Such a crystallizer is therefore characterized by "mixed suspension, mixed product removal" (MSMPR) conditions (de Jong, 1984).

The continuous MSMPR crystallizer will thus be used to generate growth and nucleation rate data. Randolph and Larson (1971) note that systems such as these have the advantage that conditions similar to those in industrial-size units can be attained. The most important advantage is that the technique permits the measurement of both nucleation and growth rates simultaneously at the same level of supersaturation, agitation, temperature, and suspension density.

In order to determine the kinetics of crystallization easily the following requirements must be met by a MSMPR crystallizer (McCabe and Smith, 1976):

1) The operation is at steady state.

2) At all times the crystallizer contains a mixed suspension with no product classification.

3) At all times uniform supersaturation exists throughout the suspension.

4) McCabe's so-called ΔL law for crystal growth applies. (Growth rate is independent of crystal size.)

5) No size-classification occurs in the product removal system.

6) No crystals are introduced with the feed.

7) The product crystals and mother liquor leave the crystallizer at equilibrium.

8) No crystal breakage into finite particle sizes occur.

If these constraints hold, the MSMPR crystallizer is said to behave ideally. For such an ideal MSMPR crystallizer the nucleation rate is constant at all points in the crystal suspension. Also, the rate of crystal growth is constant and independant of crystal size and

location throughout the suspension.

It will be noted in the following chapter 3 that CSD's obtained experimentally often differ from the results which were expected. This means that one or more of the assumptions which were made in this section is incorrect. This subject will be dealt with in Chapter 3. Chapter 4 deals with the basic nucleation mechanisms which can be present in the tungstic acid crystallization system.

3. DETERMINATION OF THE KINETIC PARAMETERS FOR CONTINUOUS CRYSTALLIZATION PROCESSES

Considerable advances in the determination of the kinetics of crystallization have been made in recent years with the help of quantitative techniques based on the population-density theory. This theory is concerned with the change in the number of particles in the various size ranges, i.e. the so called population balance theory. The population density n is defined as the limiting value

$$n = \lim_{\Delta L \to 0} \frac{\Delta N}{\Delta L} = \frac{dN}{dL} \qquad 3.1$$

where ΔN is the number of particles per unit volume in the particle-size range ΔL.

The previous chapter gave some background on the CSD in crystallizers and why this is such an important part of any crystallizing system. It was also emphasised that the CSD of a crystallizer depends on the kinetics of nucleation and growth as well as the constraints and the geometry of the system. It was said that the geometry of a crystallizing system is hard to define, and to avoid this problem a MSMPR crystallizing system was adopted. In the current chapter this MSMPR system is used to obtain the crystal nucleation and growth rate kinetics. It was mentioned above that in order to accomplish this a population balance must be set up. Such a general population balance for a MSMPR crystallizer is derived in section 3.1. Section 3.2 illustrates the calculation of the crystallization kinetics when ideal MSMPR conditions exist. In section 3.3 are four different population balances each one relating to a different non-ideal phenomenon which can occur in a MSMPR crystallizing system. Finally section 3.4 summarises the crystal growth rate model which is used to fit the non-ideal data in this dissertation to the population balance equation.

3.1 General population balance equation for a MSMPR crystallizer

The most general and useful form of the population balance equation is the macroscopic population balance equation, derived by Randolph and Larson (1971). This macroscopic population balance can be averaged in the external phase space if it is assumed that the crystallization process is carried out in a well mixed vessel.

This population balance can be used for describing transient and steady state particle size distributions in well mixed vessels.

The basic equation is:

$$\frac{\delta n}{\delta t} + \nabla.\underline{v}_i n + \frac{n d(\log V)}{dt} = B - D - \sum_j \frac{n_j Q_j}{V} \qquad 3.2$$

Where: n = Population density of the crystals.

$\underline{v}_i$ = The internal particle velocities $\underline{v}_i$ which are assumed to be a unique function of the state of the particle. An example of internal convective velocity is that of the linear rate of growth of a crystal in a supersaturated solution.

V = Total volume of the suspension.

B = Empirical birth function.

D = Empirical death function.

Q_j = The j input and output volumetric flowrates to the volume V. Q_j is taken as positive for flow out of V and negative for flow into V.

n_j = The population density of the j th stream.

If the assumption of a continuous, constant volume, isothermal, well

mixed crystallizer with mixed product removal is made, equation 3.2 can be written as:

$$\frac{\delta n}{\delta t} + \frac{\delta (Gn)}{\delta L} + D - B + n \frac{d(\log V)}{dt} = - \sum_{j} \frac{n_j Q_j}{V} \qquad 3.3$$

Where: L = The characteristic length of the particle.
G = Crystal growth rate.

This means that the only internal particle velocity that plays a part under this conditions is the linear growth rate of the particles.

This is the general population balance equation derived by deriving the population balance over a Macroscopic External Coordinate Region (Randolph and Larson, 1971).

3.2 Population balance equation for an ideal MSMPR crystallizer

If the physical assumptions mentioned in section 2.4 hold, the MSMPR crystallizer will behave as an ideal MSMPR crystallizer.

The population balance equation for an ideal MSMPR crystallizer can be developed from the general population balance equation 3.3 derived in the above section.

Assuming all the physical assumptions in section 2.4 to hold and stating that τ, the drawdown time of the vessel is V/Q_o, equation 3.3 reduces to:

$$G\frac{\delta n}{\delta L} + \frac{n}{\tau} = 0 \qquad 3.4$$

Where: Q_o = Volumetric flowrate out of the crystallizer.

Integrating equation 3.4 using the following boundary conditions; $n=n^*$ where $L=0$, results in equation 3.5:

$$n = n^* \exp\left(\frac{-L}{G\tau}\right) \qquad 3.5$$

Where: n^* = Population density of the nuclei sized crytals.

This is the population balance equation for an ideal MSMPR crystallizer.

An additional procedure to derive this same equation is discussed in Appendix F.

Determining the crystallization kinetics using this idealized population balance equation

If the natural logarithm of n is plotted against L, a straight line is obtained with slope $-1/G\tau$ and an intercept on the ordinate axis of n^* for $L=0$ as shown in figure 3.1. If the mean residence time, or drawdown time, τ is known, the rate of crystal growth rate can then be calculated.

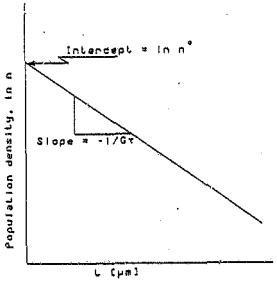

Figure 3.1 Semilog population density plot from crystallization in an ideal MSMPR crystallizer

The population density of the nuclei n° is related to the kinetics of nucleation in the following way:

Let the nucleation rate B° be defined as:

$$B^\circ = \left(\frac{dN}{dL}\right)_{L\to 0} = \frac{dN^\circ}{dt} \qquad 3.6$$

Where: N = Total number of particles per unit volume.
N° = Total number of nuclei sized particles per unit volume.

The growth rate G is defined as:

$$G = \frac{dL}{dt} \qquad 3.7$$

The nuclei population density has previously been defined as:

$$n^{\circ} = \left[\frac{dN}{dL}\right]_{L=0} \qquad 3.8$$

From simple calculus follows that:

$$\left[\frac{dN}{dt}\right]_{L=0} = \left[\left[\frac{dL}{dt}\right]\left[\frac{dN}{dL}\right]\right]_{L=0} \qquad 3.9$$

The result follows directly from combining equations 3.7, 3.8 and 3.9.

$$B^{\circ} = n^{\circ} G \qquad 3.10$$

The parameter n° therefore incorporates the nucleation kinetics. Thus the growth and nucleation rates can be determined simultaneously.

The crystallization kinetics can be obtained from an analysis of the crystal size distribution obtained experimentally for an MSMPR crystallizer operating at equilibrium. This procedure is illustrated in Appendix H.

In practice, the most important distribution is not usually the number distribution, but the mass or weight distribution. From the definition

of the population density, the total number of crystals in a unit volume of a system is given by:

$$N_t = \int_o^\infty n(L)\, dL \qquad 3.11$$

where n(L) is a function of n in terms of L.

Substituting equation 3.5 in the number distribution, equation 3.11, where the integral converges for this exponential distribution the following expression is obtained:

$$N_t = \int_o^\infty n^\circ \exp(-L/Gr)\, dL \qquad 3.12$$

$$\text{or } N_t = m_o = n^\circ Gr \qquad 3.13$$

Equation 3.13 is termed the zeroth moment of the distribution and represents the total number of crystals in the volume under consideration.

Similarly, the higher moments represent other physical quantities pertaining to the crystals in a crystallizer. The first moment is termed the specific length L_t and is the sum of the characteristic lengths of all the crystals in the distribution, as follows:

$$L_t = m_1 = \int_o^\infty L\, n^\circ \exp(-L/Gr)\, dL \qquad 3.14$$

$$= n^\circ (Gr)^2$$

The second moment multiplied with an area shape factor is the specific

surface area of the distribution, as follows:

$$A_c = k_a m_2 = k_a \int_o^\infty L^2 n^\circ \exp(-L/Gr)\, dL \qquad 3.15$$

$$= 2k_a n^\circ (Gr)^3$$

The third moment multiplied by a volume shape factor represents the specific volume of the crystals in the distribution. If this moment is also multiplied by the crystal mass density the product is the specific mass of crystals in the distribution, as follows:

$$M_c = k_v m_3 \rho = k_v \rho \int_o^\infty L^3 n^\circ \exp(-L/Gr)\, dL \qquad 3.16$$

$$= 6\rho k_v n^\circ (Gr)^4$$

Refer to Randolph and Larson (1971) for the derivation of these moments.

For the idealized MSMPR crystallizer the population balance equation has been derived as:

$$n = n^\circ \exp(-L/Gr) \qquad 3.5$$

The distribution of this population balance has only one shape. By specifying the predominant crystal size the entire distribution is defined. The development of this predominant size is summarized in Appendix J.

3.3 Population balance equation when non-ideal MSMPR conditions exists

The concept of a MSMPR crystallizer developed by Randolph and Larson (1962), has been extensively used by various investigators for the simultaneous determination of nucleation and growth kinetics in a crystallization system.

The population balance equation for an ideal MSMPR crystallizer as derived in section 3.2 has the following form:

$$n = n^{\circ} \exp (-L / G \tau) \qquad 3.5$$

When plotted as ln n against L this equation gives a straight line and most of the published data appears to follow such a law.

However, with the advent of more sophisticated particle size measurement techniques, which permit the delineation of the crystal size distribution in the near micron range, significant deviations from the ideal MSMPR model have been observed (Ramanarayanan, Athreya and Larson, 1980). Populations in this region were often found to be several orders of magnitude higher than that which was expected or could be rationalized. An illustrative example of such a phenomenon is presented in figure 3.2.

The following explanations for this non linear behavior of the data have been proposed by Ramanarayanan, Athreya and Larson (1980):

1) Classified product removal from the crystallizer.

2) Direct birth into the measured size range.

3) Growth rate dispersion exhibited by the small crystals.

4) Size dependent growth of the small crystals.

The affect of each of the above explanations on the MSMPR crystallizer kinetics will be discussed in further detail in the following sections.

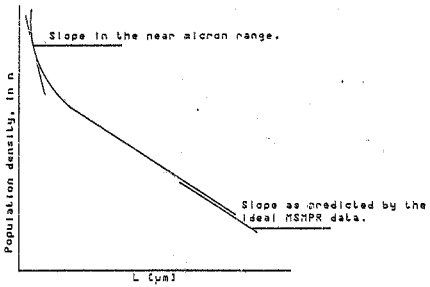

Figure 3.2 Hypothetical delineation of the semilog population density plot in the near micron range arising from the advent of more sophisticated particle size measurement techniques

3.3.1 Population balance equation when classified product removal from the MSMPR crystallizer occurs

According to Randolph (1965) classified product removal occurs when the mean retention probability of the particles vary for the various particle sizes. Removal of product-size crystals may be accelerated or retarded relative to the ideal mixed removal case, producing narrower or wider CSD's than the ideal MSMPR distribution. Such product classification can occur inadvertenzly at the point of slurry removal from a mixed suspension, or deliberately from a size-classified zone. An example of the first type is intermittent product removal from a vertical boo leg into which the larger crystals preferentially drift during the off portion of the cycle. Careful studies by, Randolph and Larson (1971), of solids removal from mixed slurries indicate that appreciable classification always occurs unless the slurry stream is removed isokinetically, i.e. at the same vector velocity as the circulating magma at the point of removal.

Deliberate size-classification can be achieved, in a mechanical sense, by several types of equipment such as elutriators, hydrocyclones, etc. If a solid-free liquor is available for counter washing, classification by elutriation can limit product draw off to essentially those crystals above a certain size. In actual practice, classification devices such as hydrocyclones can be used to preferentially remove particles larger than the classification size from the suspension, rather than removing particles less than the classification size from the product. For the purposes of deriving the population balance, a classification model shall be used which is both idealized and yet realistic, especially with respect to the previously mentioned classification devices.

The idealized model for classified product removal was described by Randolph (1965) as follows: Assume that crystals smaller than the classification size L_o are removed at a rate Q_o, while those greater than size L_o are removed at a rate zQ_o, where z is a simple constant. The flow rate Q_o maintains the liquid level in the system.

The population balance derived in section 3.1, for this case, assuming that all the requirements put forward in section 2.4 have been met, (except the second one which assumes that no product classification occurs in the system), produces the following result:

$$\frac{\delta n}{\delta t} + G\frac{\delta n}{\delta L} + h(L)\frac{n}{\tau} = 0 \qquad 3.17$$

Where: h(L) = Size dependent withdrawal rate. $h(L)=1$ for $L<L_o$
$h(L)=z$ for $L>L_o$

Solving this population balance leads to the following two results:

$$n = n^{*}\exp(-L/G\tau) \quad \text{for} \quad L<L_o \qquad 3.18$$

and

$$n = n^{*}\exp[(z-1)L_o/G\tau]\exp(-zL/G\tau) \quad \text{for} \quad L>L_o \qquad 3.19$$

The derivation of these expressions has been done by Randolph (1965).

Figure 3.3 compares the characteristic CSD form for an ideal MSMPR crystallizer with that for a classified MSMPR crystallizer. Note that in the case of the classified MSMPR crystallizer two different crystal growth rates are apparent: For small sizes up to a certain point the slope of the curve is small and therefore the growth rate large. The next part of this curve shows a larger slope and therefore a smaller growth rate. This type of behaviour will occur when z is larger than unity, i.e. more of the large crystals will be removed and the system will interpret the lack of large crystals as a slow growth rate on the part of the larger crystals.

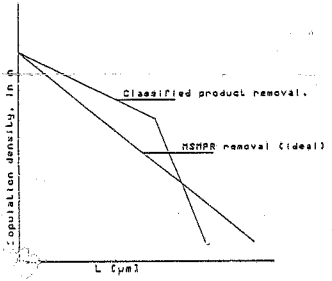

Figure 3.3 Hypothetical semilog population density plot for a MSMPR crystallizer with classified product removal

3.3.2 Population balance equation when direct birth into the measured size ranges occur

The general population balance equation 3.3 derived in section 3.1 appeared as follows:

$$\frac{\delta n}{\delta t} + \frac{\delta}{\delta L}(Gn) + n\frac{dV}{dt} + D - B = \sum_j \frac{Q_j n_j}{V} \qquad 3.3$$

Direct birth occurs when nucleation occurs because of the attrition of existing crystals in the system. Because nuclei are produced at a size other than zero, the CSD can no longer be used to calculate nucleation rates unless the variation of growth rate with crystal size is independently known. If the variation of growth rate with crystal size is not known, equation 3.3 contains two unknown functions of particle size, namely size-dependent growth rate G(L) and the birth distribution function B(L). The birth function, B(L), and the death function, D(L) are interrelated. Thus, it is patently impossible to uniquely specify both size-dependent functions B(L) and G(L) using only the single size dependent measurement n(L) without further simplifying assumptions or independent measurements. To overcome this problem, Randolph and Cise (1972), and Youngquist and Randolph (1972) have assumed that all nuclei are produced at zero size, thus B(L)=0.

For the purpose of this discussion, a steady state crystallizer with mixed product removal, liquid feeds, and a crystal system in which linear growth rate is independent of size, will be assumed. Taking this into consideration, equation 3.3 reduces to:

$$\frac{dn}{dL} = \frac{B - D}{G} - \frac{n}{Gr} \qquad 3.20$$

Randolph (1969) states that the birth and death functions, B and D

respectively, are included in the population balance to account for the fact that crystal breakage involves a loss of particles at the size broken, and a gain of particles at the size of the resultant pieces.

It is obvious from the above population balance equation that the only way to solve this equation is if expressions for the birth and death functions are presented. A complete description of these expressions are presented by Randolph (1969).

3.3.3 Population balance equation when growth rate dispersion occurs in the MSMPR crystallizer

According to de Jong (1984) there is substantial experimental evidence that, when exposed to constant external conditions of supersaturation, temperature and hydrodynamics, different crystals of the same size and of the same material can grow at different rates. This phenomenon has become known as growth rate dispersion. Most of the researchers doing work on this subject support the view that, although different crystals have different growth rates, a given crystal usually grows at a constant rate at least for periods up to a few hours. This means that size dependent growth does not occur. Another explanation for the observed non-ideal behaviour of the MSMPR crystallizer is presented by these researchers.

If growth rate dispersion occurs, the mass of crystals with high growth rates increase more rapidly than those of crystals with low growth rates. Crystals with high growth rates then contribute relatively more to the total mass, and the total increase in mass is larger than would be expected on the basis of the average growth rate. The growth rate thus appears to increase with crystal size and experimental measurements can be interpreted in terms of a size-dependent growth rate model. Any subsequent size analysis tends to separate the larger faster-growing from the smaller slower-growing

crystals, and if these size fractions are used for subsequent growth measurements, apparant size-dependent growth rates are again observed.

The causes of growth rate dispersion can be explained using the same surface integration process as will be discussed in section 3.3.4. In this case however it is assumed that different crystals have different values of s, the roughness of a crystal surface, and crystal size is not taken into account.

To modify the population balance in order to incorporate the effect of growth rate dispersion, Janse and de Jong (1976) suggest that the growth rate G must be handled as a distributed variable. These authors integrated the balance equation over the growth rate distribution to give an equation for n as a function of the average growth rate G on the assumption that G obeys a gamma distribution. The result was not very favourable since two additional parameters in the empirical expression for G were introduced. These two parameters needed to be determined experimentally which could only be done if the accuracy of the CSD measurements was great enough.

Not all the investigators working in the field of crystallization support this view of growth rate dispersion. In fact, much experimental work has been interpreted in terms of size dependent growth rates (Garside, Mullin and Das, 1974: Garside and Jancic, 1976) and several size dependent growth rate equations have been proposed (Branson, 1960; Canning and Randolph, 1967 and Abegg, Stevens and Larson, 1968) for use in combination with population balance equations in CSD modelling. A further discussion of size dependent growth rates will be presented in the following section.

3.3.4 Population balance equation when the crystal growth rates are size dependant

It is reported by Abegg, Stevens and Larson (1968) that crystal growth consists of three basic steps:

a) The diffusion of solute molecules from the bulk of the solution to the crystal-solution interface, followed by

b) a surface reaction as the solute molecules arrange themselves into the crystal lattice, and

c) the dispersion of the heat of crystallization from the crystal-solution interface back into the bulk of the solution.

According to this author the effect of the last step on the overall growth process is small in comparison with the first two steps and can be ignored.

If the growth rate is limited by the rate of diffusion through a laminar film, the growth rate is said to be diffusion-controlled. If the diffusion resistance is less than the resistance due to the surface reaction, the growth rate is reaction controlled.

It was mentioned in section 2.4 that in order for a MSMPR crystallizer to behave ideally, certain constraints must be met. One of these constraints is crystal growth rates must be size independent. Various investigators such as Abegg, Stevens and Larson (1968) have shown that this constraint is difficult to meet and the non ideal behaviour of a MSMPR crystallizer is usually the result of size dependant growth rates exhibited by the crystals.

Three mechanisms for size dependent growth have been considered by Abegg, Stevens and Larson (1968):

a) The effect of bulk or volume diffusion of solute to the crystal surface,

b) the effect of crystal size on the equilibrium solubility corresponding to that size - i.e. the so-called Gibbs-Thompson effect,

c) and the effect of size dependent surface integration kinetics.

Garside, Phillips and Shah (1976) suggest that the first two effects are unlikely to be important over the size range 1-100 μm. However, the experimental studies undertaken for the sake of this dissertation present evidence for both the first and third mechanisms.

Each of these three size dependent growth mechanisms will now be discussed more fully.

Bulk or volume diffusion

For large crystals, if the growth rate is diffusion controlled, size dependent growth rates occur. The larger crystals have a higher settling velocity and hence a greater relative crystal-solution velocity. Since the diffusion boundary layer and the diffusion resistance decrease as the velocity increases, the growth rate of the crystals in a mixed suspension will be expected to increase with increasing crystal size. This is exactly what is demonstrated in

figure 3.4: The slope of the curve decrease with an increase in crystal size and hence the crystal growth rate increase with an increase in crystal size. (The absolute inverse of the slope is proportional to the crystal growth rate as explained in section 3.2.)

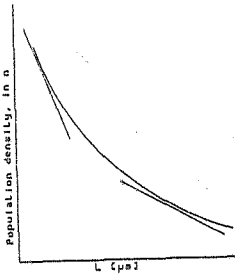

Figure 3.4 Hypothetical plot of an increasing growth rate with increasing crystal size

This bulk diffusion mechanism for large crystals does not always ensure that growth rate increases with crystal size because Bennet (1962) presented data which indicated crystal growth rates which were inversely proportional to crystal size. This phenomenon is illustrated in figure 3.5. Bennet believes that this effect is caused by classification taking place at boiling surfaces where the super-

saturation may be considerably higher than in the bulk of the crystal suspension. His views are not supported by other experimental observations and the first idea of an increasing growth rate with an increasing crystal size seems more appropriate.

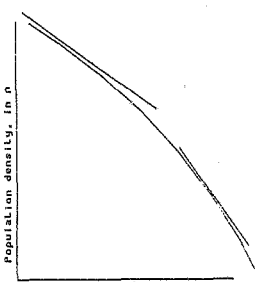

Figure 3.5 Hypothetical plot where growth rate is inversely proportional to crystal size

Garside, Phillips and Shah (1976) report that for small crystals (1-200 μm) the particle Reynolds number will be small, and as the Reynolds number tends to zero the mass transfer coefficient kd will be given by a limiting value. If growth in this region is diffusion controlled the growth rates will then increase with decreasing crystal size.

It will be shown in chapter 6 that this phenomenon of a slight increase in crystal growth rates with a decrease in crystal size, for very small crystals, does occur in the tungstic acid crystallization system studied in this dissertation.

Gibbs-Thomson effect

A complete discussion of the Gibbs-Thomson effect has been presented by Garside (1980) and Garside and Davey (1980). A brief summary of their findings is presented here:

The solubility, c_L, of a small crystal is related to its diameter, L, by the Gibbs-Thomson equation:

$$\frac{c_L}{c^*} = \exp(4M\gamma / RT\rho_c L) \qquad 3.21$$

Where: c_L=Solution equilibrium concentration for crystal size L.
c^*=Bulk solution equilibrium concentration.
M =Molecular weight.
γ =Surface energy.
R =Gas constant.
T =Absolute temperature.
ρ_c=Crystal density.
L =Characteristic crystal size.

From equation 3.21 it follows that the effect of crystal size on the solubility of a crystal is such as to increase the solubility with decreasing size. The driving force for growth, and hence the growth rate of small crystals is therefore less than that for larger crystals. The size at which this effect becomes significant depends on

the interfacial tension for the material in question. Although this is a quantity that is difficult to measure or predict with any accuracy, calculations performed by Garside (1980) using typical values indicate that the effect is unlikely to be significant for crystals larger than about 1 μm.

Surface integration kinetics

Size-dependent surface integration kinetics have been found to apply for the crystallization of potassium sulphate (Garside, Mullin and Das, 1974), potash alum (Garside, Janssen-van Rosmalen and Benneman, 1975) and nickel sulphate (Phillips and Epstein, 1974) crystals. The surface integration rates were found to increase with increasing size for all these salts and the results could be empirically correlated by a power law equation of the form:

$$G_{SI} \propto L^{Y} \qquad 3.22$$

Where: G_{SI}=Growth rate when surface integration kinetics is the limiting constraint.
L =Characteristic crystal size.
Y =0.7 for K_2SO_4 and 0.5 for both potash alum and nickel sulfate.

The observation that surface integration rates increase with an increase in crystal size, is explained as follows by Strickland-Constable (1972). Very small crystals may often be born in a near-perfect state virtually free from defects. In a multi-crystal system such as a crystallizer, the fraction of crystals of a given size containing dislocations will then increase with increasing size. Since it is easier for a rough surface to grow than a smooth surface, this leads to an increase in the average growth rate with an increase in the crystal size.

The increase in the number of dislocations with an increasing crystal size may occur for a number of reasons. Mechanical stress and the incorporation of impurity atoms into the lattice may both be important factors in initiating dislocations. In addition, the energy of crystal collisions will be greater for larger sizes and the chances of a crystal colliding with the impeller, wall or other crystals will also be greater as a result of the increasing inertia of the crystal. These more energetic collisions may increase both the amount and severity of damage to the crystal surface.

The fact that a rough surfaced crystal grows easier can be explained using the theory of Burton, Cabrara and Frank (1951) that suggests that the surface-reaction controlled growth rate of a crystal face is given by an expression of the form:

$$G = C \frac{S^2}{\sigma_c} \tanh \left(\frac{\sigma_c}{S}\right) \qquad 3.23$$

Where: G = Linear growth rate.
C = Constant.
S = Supersaturation.

And

$$\sigma_c = \frac{9.5\gamma a}{skT\lambda_s} \qquad 3.24$$

Where: γ = Surface energy.
a = Distance between growth units in crystal lattice.
s = Measure of the "roughness" of the crystal face.
k = Boltzmann constant.
T = Absolute temperature.
λ_s = Mean displacement of surface.

The value s is a measure of the "roughness" of the crystal face and Bennema and Gilmer (1973) suggested that as new dislocations are produced by mechanical stress, damage etc., the value of s may thus increase. The consequent reduction in σ_c in equation 3.24 will result in increasing growth rate G in equation 3.23 if all the other parameters in the above equation 3.23 remain constant. This appears to happen in the current tungstic acid system, and will be illustrated in section 6.4.3.

A very thorough discussion of size dependent crystal growth mechanisms has been presented here. This is necessary since it will be shown in section 6.4.3 that size-dependent crystal growth rates are the main mechanism which leads to non-ideal MSMPR crystallizer results in the present tungstic acid crystallization study.

3.4 Selection of a size dependent growth rate model

Enough evidence has been obtained from the experimental work in section 6.4.3 to be able to say with confidence that the main reason for non ideal MSMPR behaviour observed for the tungstic acid system, is because of size dependent growth rates which occur. A size dependent growth rate model must now be proposed and tested on the experimental CSD data.

Abegg, Stevens and Larson (1968) list a number of desirable properties which must be included in a realistic and useful growth rate model:

1) The growth rate model should be continuous in a region which includes L=0.

2) The growth rate model should satisfy the condition G(0)=0.

3) The zeroth moment and all positive moments of the population density distributions generated by the growth rate model should converge as discussed in section 3.2.

4) The model should be capable of fitting data which exhibit a growth rate proportional to crystal size.

Several authors have proposed empirical size-dependent growth rate models (Bransom, 1960; Canning and Randolph, 1967 and McCabe and Stevens, 1951). However, none of these models satisfy all of the above desirable properties.

A growth rate model which does satisfy all of the above points has been presented by Abegg, Stevens and Larson (1968) as follows:

$$G(L) = G^{\circ}(1+\gamma L)^{b} \qquad -1 \leq b < 1, \quad L \geq 0 \qquad 3.25$$

Where: $G(L)$ = Size dependent growth rate.
G° = Growth rate of the nuclei sized crystals.
L = Characteristic crystal dimension.
γ = $1/(G^{\circ}\tau)$, where
τ = Drawdown time of the crystallization vessel.

In addition, this model is capable of describing systems where growth rate is inversely proportional to size.

If this growth rate model is incorporated into the general population balance equation 3.3, and the only deviation from ideal behaviour is

size-dependent growth, then the steady state population distribution corresponding to this model is:

$$n = K_3 n^{\circ} (1+\gamma L)^{-b} \exp\left[- \frac{(1+\gamma L)^{1-b}}{1-b} \right] \qquad 3.26$$

Where, n = Crystal population density,
$K_3 = \exp[1/(1-b)]$
n° = Nuclei population density.
$-1 \leq b < 1$

For b=0 this model gives the same results as the ideal MSMFR crystallizing system.

Introducing two dimensionless variables y and x, where $y=n/n^{\circ}$ and $x=\gamma L$, the above population balance can be rewritten as:

$$y = K_3 (1+x)^{-b} \exp\left[- \frac{(1+x)^{1-b}}{1-b} \right] \qquad -1 \leq b < 1 \qquad 3.27$$

Plots of some of these dimensionless population distributions for different values of b are presented in figure 3.6. It is apparant from this figure that the ideal population distribution will be obtained if b=0. For b values between 0 and 1 the population distribution is such that an increase in crystal size results in an increase in crystal growth rates. For b values between -1 and 0 the growth rates are inversely proportional to the crystal size.

This proposed growth rate model 3.26 will be tested and the results presented in chapter 6.

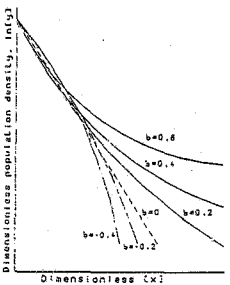

Figure 3.6 A plot of the dimensionless population density distributions for different values of b as calculated using equation 3.27

4. CRYSTAL NUCLEATION THEORIES

In order to fully define a crystallization system, the type of nucleation mechanism dominating the crystallization process must be known and expressed with an explicit expression.

Describing the nucleation and growth rates of a crystallizing system with explicit equations allows:

1. The results of experiments to be manipulated and graphed in ways that allow understanding of the crystallization process.

2. The crystallization kinetics to be incorporated into analytical scale-up and/or design procedures.

According to Randolph and Larson (1971) various investigators have shown that new crystal formation can result from one, or a combination, of the following four nucleation mechanisms: Homogeneous nucleation, heterogeneous nucleation, secondary nucleation, and attrition.

Homogeneous nucleation occurs from clear, highly supersaturated solutions when aggregates of solute molecules attain sufficient order and size to form a stable, solid particle. Heterogeneous nucleation generally refers to new particle formation resulting from the presence of foreign insoluble materials, eg. dust etc. These foreign materials provide sites where crystals can form because of reduced energy requirements. Secondary nucleation refers to nucleation induced by the presence of suspended crystals of the solute. It is to some degree similar to heterogeneous nucleation. It has alternatively been called breeding, ancillary nucleation, etc. Attrition is simply the mechanical degradation of suspended crystals in which pieces and

chips of the crystals become growing crystals. This type of nucleation is basically the same as secondary nucleation and will not be further dealt with as a separate nucleation mechanism. Each of the other three nucleation mechanisms will now be discussed in sections 4.1 to 4.3 while the effects of nucleation and growth kinetics on CSD will be illustrated in section 4.4.

4.1 Homogeneous nucleation

The fundamental expression for the rate of homogeneous nucleation was proposed as an Arrhenius-type relationship by Randolph and Larson (1971):

$$B^{\circ}=C\ EXP(-\Delta G^{*}/kT) \qquad 4.1$$

Where: B° = Homogeneous nucleation rate.
C = Proportionality constant.
ΔG^{*} = Free energy of formation of a nucleus.
k = Boltzmann's constant.
T = Absolute temperature.

The free energy of formation ΔG^{*} is the sum of a bulk and a surface contribution. It is difficult to assign a meaningfull value to this quantity because of the very small surface area of the nucleus and the virtual impossibility of measuring such quantities. Studies purporting to verify this equation generally involve calculating the surface energy from the experimental nucleation rate data and then making a judgement as to the reasonableness of its magnitude. Most results have been inconclusive, however (Randolph and Larson, 1971).

4.2 Heterogeneous nucleation

Another nucleation model has been proposed by Randolph and Larson (1971) which accounts for heterogeneous nucleation effects:

$$B^{\circ} = B_n \exp\left[-(1/kT)(16\pi\sigma^3 v/3kT\log^2 S)b\right] \qquad 4.2$$

Where: B° = Nucleation rate.
B_n = Dependent on the number of nucleus sites available for nucleation.
k = Boltzmann's constant.
σ = The surface tension.
T = Absolute temperature.
S = Supersaturation of the crystallizing solution.
b = A factor less than one.

Little success has been achieved in predicting experimental behaviour using this equation.

4.3 Secondary nucleation

Recent work attempting to characterize the nucleation phenomena in crystallizers has shown that the principal phenomenon is secondary nucleation (Larson, 1981; Desai, Rachow and Timm, 1974 and Youngquist and Randolph, 1972). Hence, much effort has been devoted to determine the mechanisms and kinetics of secondary nucleation.

Several investigators have provided insight into these mechanisms. Mason and Strickland-Constable (1966) have suggested that three types of nucleation occur in the presence of seeds. The first is initial breeding which results when dry seeds are placed in solution and when microscopic crystal dust washed from the seeds to form nuclei. The second is needle breeding resulting from the breakage of large

dendritic growths. The third is collision breeding in which nucleation is induced by collisions of seed crystals with solid surfaces. Of these, only the last is a major source of secondary nuclei in well-designed crystallizers.

Lal, Mason and Strickland-Constable (1969) were the first to demonstrate conclusively the existence of collision breeding. Using $MgSO_4.7H_2O$, KCl, and K crystals, they showed that fluid shear alone does not give rise to nucleation when a cured seed crystal is placed in a supersaturated solution. Crystal-solid contacts, however, did produce nuclei. Clontz and McCabe (1971) observed that single crystals subjected to fluid shearing forces at intermediate to low levels of supersaturation did not give rise to spontaneous nucleation, but a crystal contact was required to initiate nucleation. When a crystal collided with a surface or with a second crystal, profuse nucleation occurred. Crystal/crystal surface contacts were more fruitful than crystal/non-crystal contacts. Crystal edge collisions and sliding contacts greatly increased the number of nuclei.

Johnson, Rousseau and McCabe (1970) extended this work to show that surface roughness and hardness of the crystal face as well as the hardness of the contacting surface affect the number of nuclei produced.

These studies have shown that secondary nucleation is predominantly due to collision breeding. That is, nuclei result from the collision of seed crystals with solid surfaces, which in the case of a MSMPR crystallizer may be other crystals, impeller blades, or crystallizer surfaces.

The intrinsic mechanism for collision breeding is unknown. Powers (1963) postulated a two-step growth mechanism by which solute aggregates first diffuse to crystal surface regions and then become incorporated into the intricate lattice structure. If the lattice

incorporation step is rate determining, a surface zone of partially oriented solute aggregates develops. Upon collision this partially oriented material is displaced from the crystal mother liquor interface into the bulk of the fluid. If the size of the detached cluster exceeds the critical radius, a nucleus will be formed.

If it is assumed that collision breeding constitutes the main part of secondary nucleation, explicit equations for this secondary nucleation can then be postulated. Three different models have been proposed and each of these models will now be discussed:

A) According to Desai, Rachow and Timm (1974) if the rate of collision breeding is related to the frequency of collision, one would expect secondary nucleation to correlate with the total number of crystals within the suspended magma. Inasmuch as the critical nucleus size and the extent of aggregate orientation in the boundary layer are functions of supersaturation, supersaturation will also be a variable.

$$B^{\circ} = K_N S^s N_T^p \qquad 4.3$$

Where: B° = Secondary nucleation rate as a function of the total number of crystals in the suspended magma.
K_N = Proportionality constant.
S = Solution supersaturation.
N_T = Total number of crystals in the magma.
s and p are both kinetic orders.

B) Cayey and Estrin (1967) observed that it was necessary for seed crystals to exceed a minimum size before they became nuclei generators. Since the total number of crystals in a steady state MSMPR crystallizer is comprised principally of particles near nuclei in size, an argument exists for the investigation of other nucleation

rate models. Shor and Larson (1971) postulated that the surface of a crystal may be composed of a number of active sites, possibly formed by surface imperfections. They reasoned that a surfactant would increase the reactivity of sites, whereas an adsorbed ionic impurity would decrease such activity. Experimental observations were consistent with such a model. If it is further reasoned that the number of sites per surface area is constant, the rate of nucleation would be expected to be a function of the total interfacial crystal area as well as the fundamental mass transfer driving force, i.e. supersaturation. Their model was as follows:

$$B^{\circ} = K_A S^w A_t^k \qquad 4.4$$

Where: B° = Secondary nucleation rate as a function of the total interfacial crystal area.
K_A = Proportionality constant.
S = Solution supersaturation.
A_t = Total interfacial crystal area.
w and k are both kinetic orders.

C) The assumption that secondary nucleation is dependent upon suspension density has been made by Larson, Timm and Wolff (1968), and Rosen and Hulbert (1971):

$$B^{\circ} = K_M S^i M_t^j \qquad 4.5$$

Where: B° = Secondary nucleation rate as a function of the suspension density of the crystal magma.
K_M = Proportionality constant.
S = Solution supersaturation.
M_t = Suspension density of the crystal magma.
i and j are both kinetic orders.

Desai, Rachow and Timm (1974) showed that the model represented by equation 4.5, where the rate of nucleation is correlated in terms of supersaturation and suspended magma density, is the most appropriate model to use to express the secondary nucleation kinetics in a MSMPR crystallizer in an explicit equation. This is also the expression which will be used in this dissertation.

In many systems, j was found to be unity. It is important to note that the temperature level and the presence of foreign soluble or insoluble material can also effect all quantities and parameters in the above expression 4.5.

4.4 Effects of nucleation and growth kinetics on CSD

This section ignores the fact that crystal growth rates may be a function of a variable other than simply supersaturation. Although this is incorrect as has been proven in this dissertation, it satisfactorily serves to illustrate the effects which nucleation and growth kinetics may have on CSD.

Various empirical expressions for nucleation rates were presented in sections 4.1 to 4.3. The empirical expression usually used by Randolph and Larson (1971) for the crystal growth rate is a simple function of supersaturation;

$$G = G(S) \qquad 4.6$$

Larson, Timm and Wolff (1968) developed a power law model to aid in evaluating crystallization systems where homogeneous nucleation is the dominant source of nuclei. This system is modelled by the kinetic equations:

$$B^{\circ} = k_N S^i \quad \text{and} \qquad 4.7$$

$$G = k_G S \qquad 4.8$$

Where: B° = Crystal nucleation rate.
k_N = Proportionality constant.
S = Supersaturation of the solution.
i = Kinetic order.
G = Crystal growth rate.
k_G = Proportionality constant.

By combining equations 4.7 and 4.8 the supersaturation can be eliminated to obtain:

$$B^{\circ} = k_R G^i \qquad 4.9$$

The value of i, the kinetic order, can be found by plotting ln B° versus ln G. The model is an adequate representation of the crystallization system when the plot is a straight line. The slope is then equal to i.

When the above equation is an adequate model of the crystallization system, the crystal size is enhanced when the suspension density is increased. The lower the order of i, the greater will be this enhancement. Figure 4.1 shows typical effects of different population densities on the CSD of a crystallizer. The development of the equations relating suspension density to growth rate, nuclei size, and dominant crystal size are given in a article by Larson, Timm and Wolff (1968).

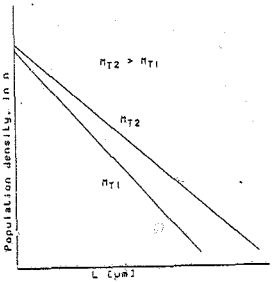

Figure 4.1 Comparison of CSD from crystallization's with different suspension densities (nonsecondary nucleation)

When secondary nucleation is the dominant nucleation mechanism in the crystallizer, the effects of both supersaturation and suspended solids must be included in the nucleation model. Such a model has been presentad in section 4.3:

$$B^{\circ} = k_M S^i M_c^j \qquad 4.5$$

Eliminating supersaturation using a linear form of the growth rate model (equation 4.8) gives:

$$B^{\circ} = k_R M_c^j G^i \qquad 4.10$$

This model tacitly assumes that nucleation occurs only in the presence of suspended solute solids.

Larson, Timm and Wolff (1968) again showed the development of the equations relating suspension density to growth rate, nuclei density, and dominant crystal size. For the case where j=1 the suspension density is linearly related to the nucleation rate. The same CSD results for different suspension densities regardless of the kinetic order of its dependency on supersaturation. This is illustrated by the parallel lines in figure 4.2.

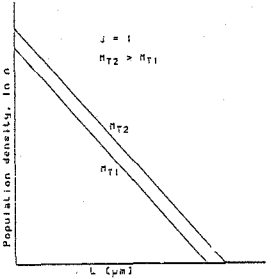

Figure 4.2 Comparison of CSD from crystallization's with different suspension densities (secondary nucleation)

For the case of $0<j<1$, the overall CSD will be enhanced by increases in suspension density. The maximum enhancement will occur as j approaches 0. For the case of $j>1$, the overall CSD will be reduced as

suspension density is increased.

It is important to do an analysis of the kinetic data for a crystallization system, since this can yield an understanding of the fundamental factors controlling the crystallization. Of equal importance is the need to determine the effect of the controllable variables upon properties desired in the product being produced in the crystallizer. Interrelationships of the independent parameters need to be determined. A designed experiment can bring to light which parameters are significant and what combination of these parameters can optimize product properties.

5 EXPERIMENTAL

This chapter has been divided in four sections: The first section describes the experimental apparatus which was used to generate the experimental data. Section 5.2 describes the reagents used in the experiments, Section 5.3 summarises the analytical techniques used to analyse the experimental results, and finally section 5.4 describes the experimental procedures adopted for the experiments.

5.1 Apparatus

Two sets of apparatus were used: An electrolytic membrane cell arrangement which converted sodium tungstate solution to a tungstic acid solution, and a MSMPR crystallizer arrangement which was used to crystallize the tungstic acid crystals out of the electrolytically produced tungstic acid solution. The first piece of apparatus was used merely to produce the liquor with which the actual crystallization experiments were performed while the second apparatus was the piece of equipment used to generate the experimental CSD data.

5.1.1 The electrolytic cell arrangement

The electrochemical cell consisted of an anode compartment separated from a cathode compartment by a cation selective membrane. The anode compartment contained a DSA 4107-4T anode plate with a TIR-2000 oxygen-evolving coating. The cathode compartment contained a stainless steel plate. The anode and cathode plates were parallel to each other and separated by a cation selective membrane. There was a gap of approximately 10mm between either of the plates and the membrane. The dimensions of both the anode and cathode plates were 20 cm long by 10 cm wide.

The cation selective membrane consisted of a physical support upon which a polymer with highly ionisable functional groups is supported. The result was a rugged sheet having ion selectivity and corrosion resistance dependent on the nature of the polymer used. The membrane used was manufactured by Ionac Chemicals (USA) and was identified as the MC-3470 type membrane. For a complete description of the chemical composition of the membrane refer to Appendix E.

The makers, Ionac Chemicals, quote the following specifications:

Electrical resistance: 0.1N NaCl = 12 Ω/cm^2 (A.C. measurement)

1.0N NaCl = 6 Ω/cm^2 (A.C. measurement)

% Perm. selectivity : 0.5N NaCl/ 1.0N NaCl = 96.2%

Ion exchange capacity: 1.22 mEq/g

Water permeability : <30 ml/hr/vt^2/5psi

Plastic turbulence promotors were used in both the anode and cathode compartments to promote the turbulence in the compartments and to ensure that the electrode plates did not contact the membrane. A Kepco power supply rectified alternating current to direct current and was used to maintain a constant electrical current to the cell.

The temperatures of the catholyte and anolyte solutions were kept constant with the use of two heat exchangers and two heaters.

The entire electrolytic cell arrangement is schematically presented in figure 5.1.

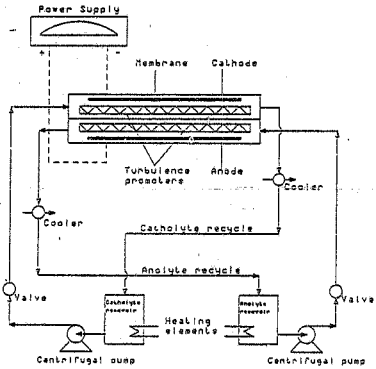

Figure 5.1 Schematic representation of the entire electrolytic cell apparatus

5.1.2 The MSMPR crystallizer

A discussion is presented in section 2.4 which justifies the use of a MSMPR crystallizer. In addition, the reason for using an evaporative crystallizer is explained by Randolph and Larson (1971). According to them, the evaporative technique is suitable for solutions which have product solubilities with small or negative temperature dependence. Since the solubility of Tungstic acid in water is very low at high and low temperatures (Perry and Chilton, 1972; Weast, 1976), the evaporative MSMPR crystallizer seemed to be the most appropriate crystallizer to use.

The solution was evaporated by boiling under atmospheric pressure because according to Stephan and Wang (1981), if the tungstic acid is produced at a low temperature the white amorphous form of metatungstic acid anhydride ($WO_3.2H_2O$) results. With a high temperature (±100 °C) the orange-yellow crystalline monohydrate ($WO_3.H_2O$) form can be produced. Since the crystalline form is the desired form it followed that boiling under atmospheric pressure is the correct way to evaporate the solution.

Basic requirements for a MSMPR crystallizer

According to Randolph and Larson (1971) certain procedures needed to be followed to meet the requirements of the idealized MSMPR crystallizer as closely as possible:

1. The crystallizer had to be well mixed.

2. The product stream had to be removed in a manner that did not change any properties from the values of the overall crystallizer.

3. The vessel had to be large enough so that adequate samples could be obtained without appreciable disturbance to the system.

4. The experiment had to be run long enough to reach steady state.

Great care was taken to try and satisfy all these requirements. The way this was done is explained in the following paragraphs:

The first requirement (uniform suspension, well-mixed) can usually be accomplished in a laboratory scale quite easily, but this becomes more difficult to achieve as the scale of size is increased. In order to satisfy the first requirement, a crystallizer with a draft tube was designed. Agitation was provided with a propeller placed concentrically in the draft tube. Vertical vanes in the annular space helped to reduce the radial motion of the circulating slurry. The draft tube is usually suitable for minimizing power input to achieve a maximum uniformity of suspension. This is very important if studies intended to determine the effects of crystal-crystal contact on nucleation rate are to be made.

The second requirement, that of obtaining a representative product stream, was important but was not always easy to obtain. Ideally the withdrawal procedure should be isokinetic. Randolph and Larson (1971) recommended the use of a withdrawal tube placed parallel to the direction of the slurry flow. Furthermore, the withdrawal velocity should reasonably match the circulation flow velocity at the withdrawal tube tip. The flow rate in the sampling tube should also be sufficient to prevent appreciable settling. Because of the small crystallizer volume and residence times chosen, the flow rate out of the crystallizer was small. Matching velocities necessitated very small diameter tubing at the withdrawal point, affecting the ability

to remove different size crystals equally. Therefore intermittent product removal was necessary. This was accomplished using conductivity probes and a vacuum withdrawal system. The vacuum withdrawal system ensured that no crystal breakage occurred during product removal as would have occurred had a pump been used.

Requirement number three stated that the volume of the crystallizer had to be adequate. According to de Jong (1984) previous investigators performed their crystallization studies in large volumed test equipment (i.e. from 1 to 100 L). Because these people used sieves to analyse the crystals and obtain the CSD of the experiment, this required large sampling volumes. According to Randolph and Larson (1971) no more than 10 % of the crystallizer contents should be removed during one intermittent product removal cycle so that residence time is not significantly changed. Because of this, very large crystallizers volumes were required in order for the system to absorb the disturbance created by taking a sample. In the present study however, a Malvern particle size analyzer was used to determine the CSD. This procedure required only small samples of the crystallizer magma with the result that the crystallizer could also be much smaller than those used by previous experimenters. Another advantage of the small crystallizer volume was that because of the high cost of tungsten smaller amounts of tungstic acid solution was required to complete each experiment.

The fourth requirement was steady state operation. According to Randolph and Larson (1971) steady state is usually attained in 10 to 15 residence times for operations where residence time is in the range of 0.25 to 1 hour. In order to satisfy this requirement the first sample was taken only after approximately ten residence times were expired.

The crystallizer arrangement

The crystallizer apparatus consisted of a one liter Pyrex glass beaker with a draft tube arrangement in it as shown in figure 5.2. This draft tube consisted of a 50mm diameter Pyrex glass tube open at both ends with four Pyrex glass vanes adhered vertically to the tube. The tube was arranged vertically in the beaker with the vanes fixed to the tube in such a way that the vanes acted as the legs of the tube. This created a spacing between the glass tube and the bottom of the beaker with the result that solution could flow in and out of the draft tube. The dimensions of the draft tube was such that the top of it was submersed in the crystallizing solution for the complete period of each run.

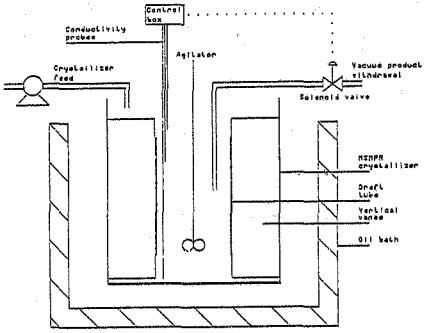

Figure 5.2 Schematic representation of the entire crystallizer apparatus

The glass beakar was immersed in an oil bath which acted as the heat source to boil the solution in the beaker and to insulate the beaker on the sides. Stirring of the solution in the crystallizer was accomplished using a glass propeller fitted concentrically in the draft tube. It forced the solution down the draft tube an up on the outside of the draft tube, between the draft tube an the wall of the beaker.

This stirrer was calibrated before use. The resulting calibration curve is shown in figure 5.3.

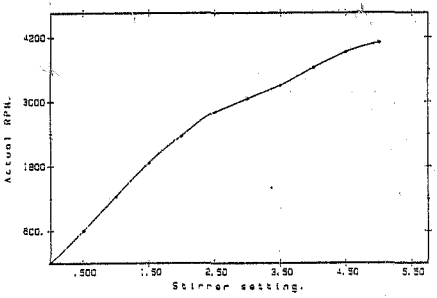

Figure 5.3 Calibration curve for the stirrer used in the MSMPR crystallizer

The level in the crystallizer was controlled with a conductivity level switch, type CA, manufactured by Terry Ferraris & C. This conductivity level control system consisted of two elements:

- A conductivity probe
- An electronic signal board.

The principle of the level control operation depended on the measurement of the electrical conductivity inside the tank to be controlled. The electrical conductivity was measured between the probe and the counter electrode as shown in figure 5.4. The system operated on two different conductivity values; one was produced during the conditions when the electrodes were immersed in air or gas, and the second in which the liquid was present between probe and counter electrode. The conductivity variation between these two conditions was measured by the probes and passed to the electronic signal board which switched the output relay, which in turn switched a two way

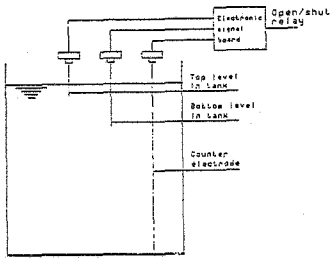

Figure 5.4 Schematic representation of the conductivity level controller in the crystallizer

direct acting solenoid valve in an open or shut position. This valve was part of the product withdrawal mechanism which enabled intermittant product withdrawal using a KNF Neuberger diaphragm vacuum pump.

The solid-free crystallizer feed containing dissolved tungstic acid was pumped into the crystallizer using a variable speed, H. R. Flow-inducer type MHRE, peristaltic pump. This peristaltic pump was calibrated before using it. The calibration was done using a typical tungstic acid solution at a constant room temperature of 25 °C. The resulting calibration curve is presented in figure 5.5.

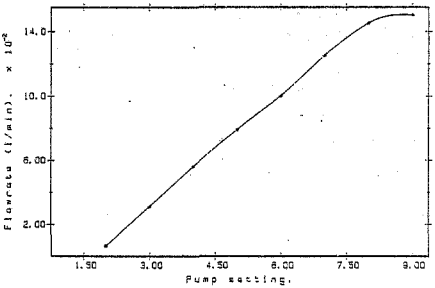

Figure 5.5 Calibration curve for the variable speed peristaltic pump used to pump the tungstic acid solution into the MSMPR crystallizer

5.2 Reagents

Initially sodium tungstate solutions acquired from Board Hardmetals (Pty) Ltd were used. These solutions contained impurities such as molybdenum, silica, phosphorus, arsenic, and chlorides. All these impurities, except the chlorides, could be removed using the methods described in Appendix A.

The presence of the chlorides posed a problem that would not have been present had the soda ash pressure leaching process been used to produce the sodium tungstate.

According to Comey and Hahn (1921) the solubility of tungstic acid in water increases dramatically in the presence of chlorides. The result was that no tungstic acid crystals could be formed in a reasonable time in the evaporative MSMPR crystallizer because of the high equilibrium solubility in the presence of chloride ions.

Realising that this problem would not arise using solutions from a soda ash pressure leaching process, it was decided to prepare sodium tungstate solutions that were free of chlorides, and for that matter, free of any other impurities. Besides the fact that no chlorides would be present, this procedure also aided to achieve reproducible crystallization results.

Preparation of sodium tungstate solution

The preparation of such a pure sodium tungstate solution was done as follows:

Pure ammonium paratungstate crystals were obtained from Boart

Hardmetals (Pty) Ltd. These crystals were dissolved in a stoichiometric excess amount of hot caustic soda solution. The following reaction occurred:

$$2NaOH + (NH_4)_2WO_4 \rightleftharpoons Na_2WO_4 + 2NH_4OH \qquad 5.1$$

The resulting ammonium hydroxide in solution dissociated to form ammonia and water and the ammonia was then driven off by boiling the solution.

$$NH_4OH \rightleftharpoons H_2O + NH_3\uparrow \qquad 5.2$$

Any residual ammonia in the sodium tungstate solution entered into the electrolytic cell along with the sodium tungstate. Here it was either driven off because of the heat of the solution or it was transported across the membrane in the form of NH_4^+ ions along with the Na^+ ions.

A very dilute caustic soda solution was used as the catholyte solution in the electrolytic cell arrangement and a very dilute hydrochloric acid solution was used to wash the crystals obtained from the crystallizer.

5.3 Analytical techniques

The various analytical techniques used are described below.

5.3.1 Analysis of the Na and W contents in the electrolytic cell

During the production of the tungstic acid solution in the electrolytic membrane cell the Na:W ratio in the anode had to be closely monitored in order for this ratio not to drop below a certain preset level. This was done for reasons that will be discussed in section 6.1.3. These analyses of the sodium and tungsten concentrations in the anode were done using an Atomic Absorption machine.

5.3.2 Determination of the specific gravity of the tungstic acid crystals

The specific gravity (S.G.) of the tungstic acid crystals produced in the crystallizer had to be measured. This was done using a liquid pychnometer. The following procedure was followed (Fourie, 1983):

1. Measure the weight of the dry S.G. bottle. (A)

2. Fill the dry S.G. bottle with water, allowing no air bubbles to be present, and measure the weight of this configuration. (B)

3. Dry the S.G. bottle, put in the tungstic acid sample and weigh again. (C)

4. Fill the bottle containing the tungstic acid sample with water, with no air bubbles present and weigh. (D)

The calculation of the S.G. is then as follows:

$$S.G. = \frac{C-A}{(C+B)-(A+D)} \qquad 5.3$$

5.3.3 Determining an X-ray diffraction pattern for the tungstic acid crystals

An X-ray diffraction pattern of the tungstic acid crystals was obtained. This was done because according to Reed-Hill (1968) X-ray diffraction patterns can be used to determine whether a substance is crystalline or not.

5.3.4 Determining the CSD for each experimental run

Representative samples of the crystalline material suspended in solution were taken from the MSMPR crystallizer after approximately ten crystallizer residence times, whereafter steady state conditions could then be assumed (Randolph and Larson, 1971).

The volume of the slurry sample was measured and the sample was then immediately filtered using a pressure filter. The crystals were then resuspended in a slightly acidified distilled water solution. This prevented redissolving of the crystals or further growth of the crystals. It did not matter that the crystals were suspended in a different volume of a different liquid because the samples were analysed using a Malvern Particle Sizer 3600 E type and the results were presented as % mass fractions in the different size fractions. An example of such a result sheet is presented in section 6.3.

5.4 Experimental procedures

5.4.1 Operation of the electrolytic cell

The anolyte solution consisted of a pure sodium tungstate solution containing small amounts of ammonium hydroxide. The preparation of

this solution was discussed in section 5.2. The catholyte solution was a diluted caustic soda solution. Both the anolyte and catholyte solution volumes was initially 6 L.

Before the cell operation was started, the cation selective membrane needed to be thoroughly wetted. This was accomplished by pumping the anolyte and catholyte solutions through the cell for approximately one hour. The temperatures of both the anolyte and catholyte solutions were heated up to a constant temperature of 30 °C.

After this the amount of sodium in the anolyte was determined and the current density chosen. The time needed to convert all the sodium ions across the membrane was then calculated using Faraday's equation. (Refer to Appendix C for a short summary of this equation.) Only after all these procedures were completed was the cell operation started.

During the cell operation frequent samples of the anolyte solution were taken in order for the Na:W ratio in the solution to be monitored.

After the desired Na:W ratio had been obtained (approximately 1:80 by mass) the cell operation was stopped, and the resulting tungstic acid solution transported to a container from where the crystallization part of the operation took place.

5.4.2 Operation of the MSMPR crystallizer

The tungstic acid solution produced in the electrolytic cell was stored in a 25 l glass storage container. The solution temperature was kept constant at 30 °C and the solution was continuously stirred. From here the solution was continuously pumped into the crystallizer using a variable speed peristaltic pump. Different flowrates were used for

different experimental runs. Great care was taken to ensure that the solution going into the crystallizer contained no tungstic acid crystals. In the crystallizer the solution was stirred continuously using the glass stirrer in the draft tube.

The tungstic acid solution in the MSMPR crystallizer was heated for a sufficient length of time until it reached a constant boiling temperature of 95°C after which the seed crystals were introduced into the crystallizer. The introduction of seed crystals at the beginning of the run was done once only for each run. Seed crystals were necessary since no crystallization occurred in the crystalizer if no initial seed crystals were added. A constant amount of 0.1 g seed crystals, with a constant CSD, was introduced in each of the runs. After the introduction of the seed crystals the crystallizer system was left undisturbed for a duration of at least ten residence times before sampling of the crystallizer contents was conducted.

Yellow tungstic acid crystals were formed in the crystallizer. According to Stephen and Wang (1981) the monohydrate, $WO_3.H_2O$, will be formed if the crystallization temperature is approximately 100°C. According to Perry and Chilton (1972) this monohydrate of tungsten has either a rhombic or an orthorhombic crystal structure with a specific gravity (S.G.) of 5.5.

The liquid level in the crystallizer was controlled using the conductivity probes in the beaker which activated a relay valve in the product removal line in an open or shut position. The product removal line was connected to a vacuum line with which the product was removed from the crystallizer. The product removed from the crystallizer was stored in another 25 l glass storage container.

Samples from the crystallizer were taken manually using a piece of tubing with the same diameter as the product removal line. The diameter of this line was such that the vector velocity inside the

product removal line was approximately the same as that inside the crystallizer. This diameter was obtained experimentally and the diameter used for the sake of the experiments was 8 mm. Using a separate piece of tubing for the samples ensured that no dead volumes occurred in the sampling volume which helped to improve the reliability of the samples.

The heat source for the crystallizer was an oil bath. The temperature of this oil bath was kept constant during a run by means of a heating coil with a temperature controller connected to it. The variance of this oil bath temperature during a run was negligibly small.

Various runs were conducted with various different conditions. All the data are presented in Appendix C.

6 EXPERIMENTAL RESULTS

This chapter summarises all the experimental results obtained from the various experiments conducted for the purpose of this dissertation. Section 6.1 describes an experiment using the electrolytic membrane cell operation which was conducted to determine the membrane efficiency of the cation selective membrane for the electrolytic removal of sodium from sodium tungstate to produce dissolved tungstic acid. Section 6.2 briefly summarises the experiments which were used to investigate the crystallization of the tungstic acid crystals from solution. It is concluded that the specific gravity of the crystals produced is close to that of the tungsten monohydrate, $WO_3.H_2O$. It is also shown that an X-ray diffraction pattern exists for these crystals which indeed proves that the material is crystalline.

Section 6.3 explains the method used to calculate the CSD for each crystallization experiment which was conducted. It is shown that the assumption of a spherical shape for the crystals is justified. Section 6.4 investigates the possible causes for the non-ideal behaviour of the MSMPR crystallizer, and it is concluded that size dependent growth of the crystals is the main reason for this behaviour. The subsequent size dependent growth rate model to be incorporated in the population balance equation to account for this non-ideal behaviour is then summarised in section 6.5 and the fitting of this model to the experimental data is discussed. The joint confidence region for the two parameter growth rate model is calculated in section 6.6. Section 6.7 discusses the major nucleation processes apparent in the current crystallization system, and come to the conclusion that secondary nucleation is the dominant nucleation mechanism in this system. The behaviour of the crystallization system with varying experimental conditions is discussed in sections 6.8 and 6.9 and the empirical expressions used to describe the nucleation and growth kinetics are derived in section 6.10.

6.1 Electrolysis of dissolved sodium tungstate to produce dissolved tungstic acid

Experiments were conducted which involved the production of tungstic acid solution in the electrolytic membrane cell, and then involved crystallization of pure tungstic acid crystals in the MSMPR crystallizer.

An experiment was performed which permitted calculation of the membrane efficiency of the electrochemical cell for transporting sodium ions from the sodium tungstate anolyte solution across the cation selective membrane to the caustic soda catholyte solution. This experiment is described in section 6.1.1. The change in voltage drop during the experiment reported in section 6.1.1 is described in section 6.1.2.

It was observed that tungstic acid solids were formed in the electrolytic cell if the cell was run for a sufficiently long period of time. These solids were amorphous and a nuisance in the efficient working of the cell. This problem was overcome by regulating the sodium content in the anolyte solution. Section 6.1.3 has a complete description of this aspect.

6.1.1 Membrane efficiency for the electrolytic removal of sodium from sodium tungstate using a cation selective membrane

Figure 6.1 shows a plot of sodium ion concentration in the catholyte versus time during electrolysis in the electrolytic membrane cell. The raw data for this run is presented in Appendix L. This plot shows that that there are two distinct regions present. Initially, sodium flux is constant at a membrane efficiency of 69%. At a catholyte Na^+ concentration of around 12 g/l the flux drops very rapidly to a constant value corresponding to a membrane efficiency of approximately

18%. Refer to Appendix D for definitions and details concerning the calculations of these membrane efficiencies.

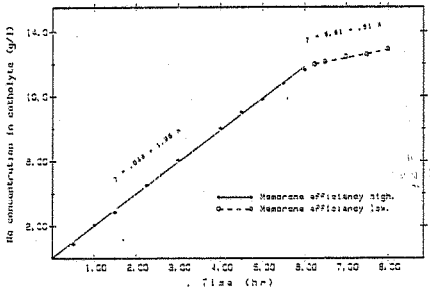

Figure 6.1 Plot of sodium ion concentration in the catholyte versus the electrolysis time in the electrolytic membrane cell. Refer to Appendix L for the data which was used to construct this plot

A possible explanation for the observation of two distinct membrane efficiency regions is that the transition from a high to a low membrane efficiency occurs at the point where nearly all the sodium

ions have been transported across the membrane and the dissociation of water becomes excessive. From the experimental data in Appendix L it is seen that this might be the case because the Na^+ concentration in the anode compartment dropped below 2 g/l in the low efficiency region.

Previous investigators, Verbaan, Greenslade and Wade (1984), reported membrane efficiencies for the removal of Na from Na_2WO_4 as high as 80%. In their case the anode solution had only one cation species, Na^+, and not two as in the present case where both Na^+ and a small amount of NH_4^+ were present. The reason for the presence of this second species has been explained in section 5.2. In this case both the cation species may have been simultaneously transported through the membrane with the result that the net membrane efficiency for the Na flux was lower than expected.

6.1.2 Voltage drop across the cell

Figure 6.2 shows the observed voltage drop across the cell during the electrolysis experiment reported in section 6.1.1:

Initially the voltage drop decreased as the run proceeded and then it reached a minimum value before increasing again. The decrease in voltage drop could be attributed to an increase in the initially low catholyte concentration since the electrical resistance of the cell is governed largely by the conductivity in the anolyte and catholyte compartments. The increase in voltage drop may have been the result of the decrease in the amount of available cations in the anode solution.

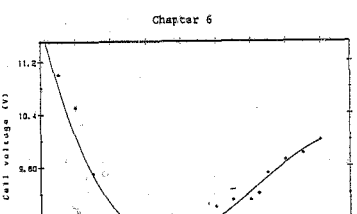

Figure 6.2 Plot of observed voltage drop across the cell versus the electrolysis time in the electrolytic membrane cell. Refer to Appendix L for the data which was used to construct this plot

6.1.3 Effect of residual anolyte sodium ion concentration on the precipitation of amorphous tungstic acid during electrolysis of sodium tungstate to form dissolved tungstic acid solution

Soluble tungstic acid is formed in the anolyte when Na^+ ions are removed from the sodium tungstate solution and transported across the membrane. (Refer to Appendix B for a description of the chemistry in the cell.) The tungstic acid formation resulted in a rapid pH drop until it reached a point where the tungstic acid started to precipitate in the cell circuit.

The precipitation of such amorphous tungstic acid in the cell circuit was undesirable, so the concentration of Na^+, relative to the tungsten concentration in the anolyte solution was checked so that the solution could be removed before the $[Na^+]$ to $[W^{6+}]$ ratio dropped too low. This ratio was in the order of approximately 1:80 g/l. The residual sodium ions were present as Na_2WO_4, which did not play a part in the subsequent crystallization of H_2WO_4 in the MSMPR crystallizer.

6.2 Crystallization of the tungstic acid solution

After the production of the tungstic acid solution in the anode compartment of the electrolytic cell it was transferred to a storage container from which the continuous feed to the MSMPR crystallizer was pumped using a peristaltic pump.

The tungstic acid solution in the MSMPR crystallizer was heated for a sufficient length of time until it reached a constant boiling temperature of 95°C after which the feed crystals were introduced into the crystallizer. The introduction of feed crystals at the beginning of the run was done once only for each run.

Feed crystals were necessary since no crystallization occurred in the crystalizer if no initial seed crystals were added. A constant amount of seed crystals, with a constant CSD, were introduced in all the runs. This constant amount was 0.1 g.

Yellow tungstic acid crystals were formed in the crystallizer. According to Stephen and Wang (1981) the monohydrate, $WO_3.H_2O$, will be formed when the crystallization temperature is approximately 100°C. According to Perry and Chilton (1972) this monohydrate of tungsten has either a rhombic or an orthorhombic crystal structure with a specific gravity (S.G.) of 5.5.

The S.G. of the formed material was determined with the method described in section 5.3. The S.G. of the material was found to be 5.6 which was close to the literature value of 5.5 if experimental error is taken into account. This indicated that the tungstic acid formed was indeed in the monohydrate form. In addition to this, the yellow tungstic acid material formed in the crystallizer was tested to see

whether it was crystalline, and to see if it was the ortho-tungstic acid crystalline form that was formed. This was done by using the X-ray diffraction method described in section 5.3.

The results obtained using this X-ray diffraction method was as follows: X-ray diffraction patterns were found. The set of interplanar spacings that was calculated was exactly those of the monohydrate, $WO_3.H_2O$. Figure 6.3 is a plot of the intensity of the X-ray reflections versus the interplanar spacings. Both the X-ray Diffraction Data Index and the experimental interplanar distances are presented in table 6.1.

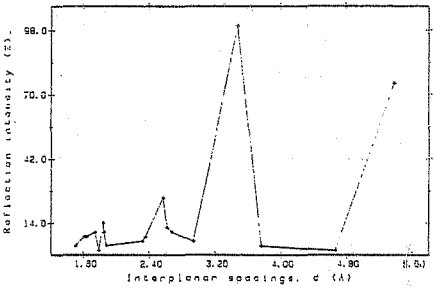

Figure 6.3 Intensity of the X-ray diffractions versus the interplanar spacings in the tungstic acid crystals produced in the MSMPR crystallizer

Data Index		Experimental	
d (A°)	I/I_1	d (A°)	I/I_1
5.39	75	5.40	75
3.86	2	3.86	2
3.49	100	3.48	100
2.95	6	2.94	6
2.687	10	2.68	10
2.626	12	2.6	12
2.570	25	2.57	25
2.360	8	2.36	6
2.322	6	2.32	8
1.979	4	1.98	4
1.875	4	1.88	5
1.854	10	1.85	11
1.837	14	1.836	14
1.739	10	1.74	14
1.637	8	1.64	10
1.611	8	1.61	8
1.504	4	1.50	4
1.211	2	1.21	2

Table 6.1 Comparison between the experimentally obtained interplanar distances and the values from the X-ray diffraction data for tungstic acid crystals.

These results indicated that the product from the MSMPR crystallizer was indeed crystalline tungsten monohydrate, or tungstic acid. These crystals were in the form of $WO_3.H_2O$ and this indicated that calcining the crystals would ensure the formation of tungsten oxide, WO_3, an intermediate in the production of tungsten metal powder.

6.3 Calculating the CSD for each run

Representative samples of the crystalline material were taken from the MSMPR crystallizer after approximately 10 crystallizer residance times as steady state conditions could then be assumed.(Section 5.1.2.)

The sample solution was immediately filtered using a pressure filter, and the crystals resuspended in a slightly acidic distilled water solution. This prevented, redissolving of the crystals or further growth of the crystals. It did not matter that the crystals were suspended in a different volume of liquid since the samples were analysed using a Malvern Particle Sizer 3600 E type and the results were presented as % mass fractions in the different size fractions. An example of such a result sheet is presented in table 6.2. The rest of the raw data, for the different runs, are presented in Appendix G.

USER EXPERIMENTAL AND SAMPLE DETAILS

2048||A
R18 ! 22H30

RESULTS

RUN NUMBER= 10 TIME=01-28-10 LOG DIFFERENCE= 5.08

SAMPLE % VOLUME CONCENTRATION= 0.0277 BEAM OBSCURATION= 0.21

SIZE MICRONS	WEIGHT % UNDER	WEIGHT IN BAND MICRONS		%	LIGHT ENERGY CALCULATED	LIGHT ENERGY MEASURED
118.4	100.0					
54.9	100.0	118.4-	54.9	0.0	92	40
33.7	100.0	54.9-	33.7	0.0	167	127
23.7	99.9	33.7-	23.7	0.1	272	241
17.7	99.8	23.7-	17.7	0.1	426	404
13.6	94.1	17.7-	13.6	4.2	665	658
10.5	82.1	13.6-	10.5	12.7	1001	993
8.1	54.7	10.5-	8.1	27.4	1432	1440
6.3	20.5	8.1-	6.3	34.2	1853	1852
4.8	4.0	6.3-	4.8	16.5	2047	2047
3.7	1.5	4.8-	3.7	2.5	1951	1853
2.8	1.0	3.7-	2.8	0.5	1452	1369
2.2	0.4	2.8-	2.2	0.7	1186	1135
1.7	0.0	2.2-	1.7	0.4	1292	1304
1.3	0.0	1.7-	1.3	0.0	1414	1552
1.0	0.0	1.3-	1.0	0.0	1596	1265

Table 6.2 An example result sheet for the Malvern 3600 Particle Size analyser in which the mass fractions of crystals in the different size ranges are presented

The suspension density of the crystalline solution was determined for each experiment. This was done using part of the sample that was taken from the crystallizer. The solution was filtered, the weight of the dry crystals determined and the volume of filtrate measured. The suspension density was then calculated.

A volume shape factor had to be determined for the crystals. Electron microscope photographs were taken of the crystals and it was found that most of the crystals had a spherical shape as shown in figure 6.4. A spherical shape was thus assumed for the crystals.

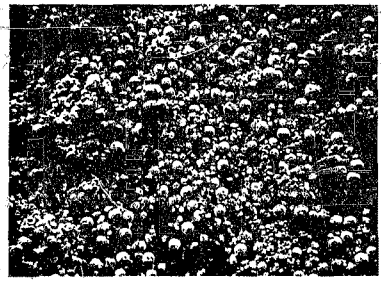

Figure 6.4 Electron microscope photograph of the tungstic acid crystals confirming the roundness of the crystals (Magnification x 150)

A description of the calculation of the crystal population density for each size fraction is presented in Appendix H. In order to calculate this population density for each size the following unknowns had to be determined experimentally:

k_v, the shape factor

ρ, the absolute density of the crystals

ΔW, the weight fraction of crystals in the size range L_1 to L_2

M_T, the suspension density of the crystallizer magma.

All these values were calculated and the crystal population density for each size fraction could then be calculated and plotted versus the crystal size, for each experiment. The resulting population density data for all the experimental runs are presented in Appenix I. An example of such plots is shown in figura 6.5.

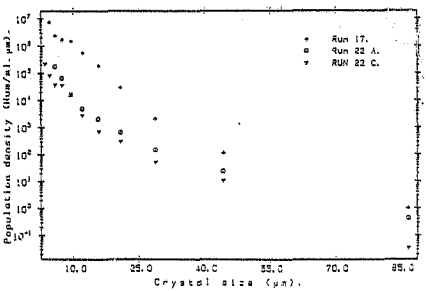

Figure 6.5 Semilog plot of crystal population density versus the crystal size for runs 17, 22A and 22C. Refer to Appendix G for the experimental conditions of these runs

The plots of population density versus crystal size for various experiments can be interpreted to establish the nucleation kinetics and crystal growth kinetics as discussed in Chapter 3.

6.4 Interpreting the experimental CSD's to determine the nucleation and growth kinetics of the tungstic acid crystallizing system

The population balance equation for an ideal MSMPR crystallizer, where growth rate is size independent, was shown in section 3.2 to be as follows:

$$n = n^{*} \exp(-L/Gr) \qquad 6.1$$

If the assumption of ideal conditions as defined in section 2.4 holds, a plot of ln n versus L should give a straight line.

From the experimental results presented in figure 6.6 it is evident that non-ideal conditions must exist since the plot of ln n versus L is curved and not linear. The curvature of the plot indicates that the crystal growth rate is not a constant value for the complete size range of the crystals. It is observed that the growth rate is proportional to the absolute inverse of the slope of the curve, and that the slope decreases with an increase in crystal size. This means that the crystal growth rate increases with an increase in crystal size. The data for the experimental results plotted on figure 6.6 are presented in Appendix I.

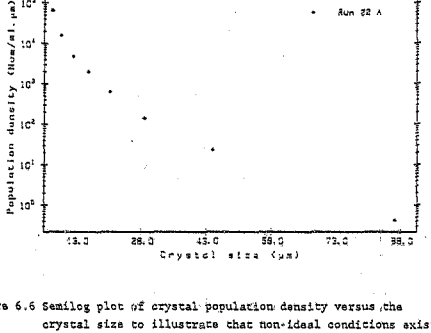

Figure 6.6 Semilog plot of crystal population density versus the crystal size to illustrate that non-ideal conditions exist in the MSMPR crystallizer.
Run 22A: τ=78.6min, M_T=0.97g/l, S=13.1g/l.

As discussed in section 3.3, one of four explanations for this trend in crystal growth rate can be proposed:

6.4.1 Classified product removal from the crystallizer

As discussed in section 3.3, the observation that crystal growth rate increased with an increase in crystal size could be explained if classified product removal occurred in the system.

In the experimental apparatus great care was taken to prevent classified product removal from taking place. Refer to section 5.1.2 for a complete description of the efforts made to prevent classified product removal.

6.4.2 Direct birth into the measured size range

According to Randolph and Larson (1971) the present system under considaration (i.e tungstic acid in water) is a class I type crystallizing system.

This means that the per-pass yield of the crystallizer is low and depends on the throughput through the crystallizer. The resulting crystal growth rate will be low and according to Garside and Davey (1980) the lower the growth rate, the smoother the crystal-solution interface and the less amount of needle-like dendritic growths take place on the surface.

In section 3.3 it was explained that direct birth into the measured size range occurs because of the attrition of needle-like dendritic growths from the surface of the crystals. Thus, if the amount of needle-like dendritic growths are minimized, no direct birth into the measured size range occurs. Furthermore, the maximum crystal size in this system is approximately 85μm, which again minimizes the probability that large secondary nuclei are produced in the measurable size range.

If the preceding discussion holds, it can be assumed that no secondary nuclei are born in the size range 2-20μm, and the observed effect that crystal growth rate is a function of size can be attributed only to either size dependent growth kinetics or growth rate dispersion.

6.4.3 Size dependent growth kinetics

It is difficult to decide which of the last two possible explanations apply to the system under consideration. (i.e. Size dependent growth kinetics or growth rate dispersion.)
In the following discussion an attempt is made to explain why the former of the two explanations is assumed to be the most likely cause why the growth rate is a function of crystal size.

From the results presented on figure 6.7 it is noted that for a crystal size up to about 25μm, the curves are almost linear (slightly curved downward) and obey McCabe's ΔL law. According to Abegg, Stevens and Larson (1968) this is to be expected because with very low relative crystal solution velocities, the rate of diffusion is probably the limiting factor. In section 3.3 it was predicted that if diffusion is the limiting factor for small crystals, an opposite trend as what usually could be expected would have been noted, i.e. the crystal growth rate decreases with an increase in size. (Note that for small crystals the mass transfer coefficient increases with a decrease in crystal size.)

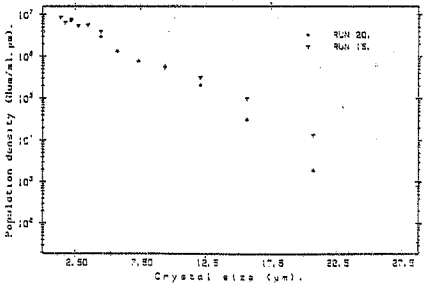

Figure 6.7 Plots of ln n versus crystal size to illustrate the phenomena that size dependent growth kinetics is the dominating factor in the present tungstic acid crystallization system. Run 15: τ=48.6min, M_T=18.6g/l, S=41.2g/l. Run 20: τ=51min, M_T=12.1g/l, S=26.8g/l. Refer to Appendix G for the experimental conditions of these runs

Careful examination of figure 6.7 shows exactly this trend: For small crystal sizes up to about 25μm the curves are slightly curved downward with the result that the growth rates decrease slightly with size. This presents evidence that bulk diffusion is the limiting factor for crystal growth for crystal sizes up to approximately 25μm.

When the crystals exceed 25μm the relative crystal-solution velocity must have increased sufficiently so that diffusion ceases to be the limiting factor and surface integration kinetics become the limiting factor. This can be deduced because the growth rates in figure 6.6 start to increase with an increase in crystal size from approximately 25μm.

Further experimental evidence showing that the increase in growth rate with crystal size occurs because of an increase in the dislocation density of the crystals, is given by electron microscope photo's taken of the crystals. From figures 6.8 and 6.9 it can be observed that the smaller crystals have a much lower dislocation density than the larger ones, and this corresponds with the theory presented in section 3.3.

The first observation, that of diffusion resistance, is not very important because the curves are fairly close to straight lines in comparison to the second part of the curve where surface reaction becomes important. Thus, the first part of all the curves shall be handled as if it were obeying McCabe's ΔL law (Abegg, Stevens and Larson, 1968).

The observation that both diffusion and surface reaction can be apparent is not a new concept. Rumford and Bain (1950), in studying the crystallization of NaCl found their system to be either diffusion or reaction controlled, depending on the system conditions.

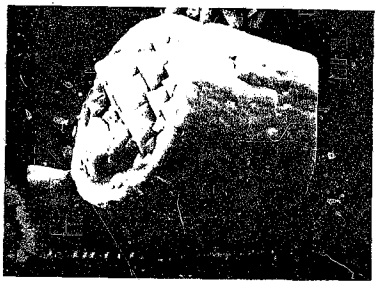

Figure 6.8 Electron microscope photograph of a fairly small crystal (<20μ). Crystal obtained from Run 17.

Figure 6.9 Electron microscope photograph of a fairly large crystal (>40μ). Crystals obtained from Run 17.

6.4.4 Growth rate dispersion

As discussed in the previous section it is assumed that growth rate dispersion had no influence in the growth rate dependence on crystal size. Some experimental evidence as presented in the preceding section exists to prove that size dependent growth kinetics do play a role in the observed trends, but there is no evidence to prove that growth rate dispersion does not play a part in the system. Taking this into account, the assumption that growth rate dispersion does not play a part in this tungstic acid system must be accepted with caution. More experiments will have to be performed to be able to ignore the effect of growth rate dispersion.

6.5 Modelling of the size dependent growth rate

Because the crystal growth rate is significantly size dependent, the product size distribution differs significantly from that predicted by the ideal population balance equation 3.2 discussed in section 3.2. In the derivation of this ideal population balance equation, size-independent growth rates were assumed. Obviously, in order to correctly predict and analyze the experimental size distributions, a size-dependent growth rate expression is required.

The mathematical expression for size-dependent growth rate, and the resulting population balance equation which will be used, has been derived and discussed in section 3.3 and for the sake of convenience is reproduced as follows:

$$G(L) = G^{\circ}(1+\gamma L)^{b} \qquad -1 \leq b < 1, \quad L \geq 0 \qquad 6.2$$

$$n(L) = K_3 n^{\circ}(1+\gamma L)^{-b}\exp\left[-\frac{(1+\gamma L)^{1-b}}{1-b}\right] \qquad 6.3$$

where: $K_3 = \exp\left(\frac{1}{1-b}\right)$

$$\gamma = \frac{1}{G^{\circ}\tau}$$

According to Ramanarayanan, Athreya and Larson (1980) the nuclei population density n° and G°, the growth rate of these small crystals, asymtote towards the y-axis, with the result that these two values can be treated as parameters along with the parameter b. The size-dependent growth rate model was thus first of all treated as a three parameter model. Least square fits of this proposed growth rate model to the data for all the experimental runs were done, and the following conclusion was reached: For all the experimental runs the value of the parameter b was approximately the same. Remembering that this value of b should only be a function of the type of system, and not of the specific system conditions, a constant average value of b for all the runs was assumed and the growth rate model treated as a two parameter model, with n° and G° being the two parameters.

The average of the different b values for all the experimental runs was calculated and taken as the value of b for the tungstic acid system. A constant average value of b=0.58 was assumed and used in the growth rate model. The fitting of this growth rate model to the experimental GSD data was then done as follows:

Section 6.4.3 contains a discussion of why it can be assumed that McCabe's ΔL law holds to an extent for small sizes in the system under consideration. Thus the first part of all the experimental plots of ln n versus L should result in a straight line with a slope equal to $-1/G^{\circ}\tau$ and an intercept equal to the logarithm of the nuclei density n°. The correctness of this assumption was not very important since it was only used to predict initial values for G° and n°.

Using these initial values for n^* and G^*, and the constant value of b=0.58, a trial and error procedure was used to determine the values of n^* and G^* which gave the best least squares fit of the dimensionless population distribution defined by equation 3.27 to each of the different experimental CSD's.

The Fortran program calculating the two parameters n^* and G^*, with b as a constant value of 0.58, for the best least squares fit of the model to the data is presented in Appendix M, together with a discussion of the procedure which the program follows.

The resulting model which was found to fit the data reasonably well and which can thus be used to predict the size-dependent crystal growth rates in a tungstic acid crystallizing system can be expressed as follows:

$$G(L) = G^*(1+\gamma L)^{0.58} \qquad -1 \leq b < 1 \qquad 6.2$$

$$L \geq 0$$

Where: $$\gamma = \frac{1}{G^* \tau}$$

and the values of G^*, n^* and τ are dependent on the specific system conditions that exist.

Using this growth rate model enables the calculation of the nucleation rate as well because according to Abegg, Stevens and Larson (1968) the value of B^*, the nucleation rate, for size-dependent crystal growth rates is given by $n^* * G^*$ and both these values have been determined in using the size-dependent growth rate model.

Figures 6.10 to 6.12 compare some of the experimental results and the corresponding values predicted by the size dependent growth rate model. The experimental data and model expressions for these runs together with all the other runs are presented in Appendix I.

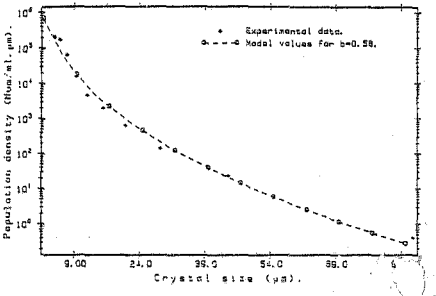

Figure 6.10 Comparison between the experimental data for Run 22A and the results obtained from using the growth rate model given by equation 6.2 with fitted values of n°=7.0E6 number/ml.μm and G°=1.05E-2 μm/min. (r=78.6min M_T=0.97g/1 and S=15.1g/1.)

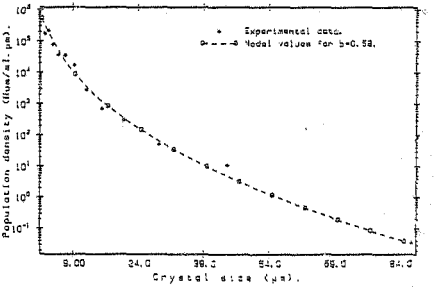

Figure 6.11 Comparison between the experimental data for Run 22C and the results obtained from using the growth rate modal given by equation 6.2 with fitted values of n°=8.5E6 number/ml.μm and G°=8.0E-3 μm/min. (r=78.6min, M_T=0.47g/1 and S=16.1g/1.)

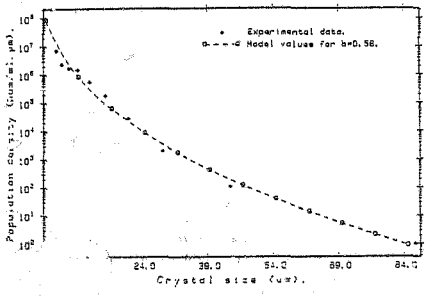

Figure 6.12 Comparison between the experimental data for Run 17 and the results obtained from using the growth rate model given by equation 6.2 with fitted values of n°=2.5E9 number/ml./μm and G°=7.0E-3 μm/min. (τ=67.5min, M_T=41g/l and S=57.5g/l.)

6.6 Joint confidence region for the two parameter model

With b given a constant value of 0.58, the sensitivity of the growth rate model towards n° and G° was examined.

It is possible to show that confidence regions for different probabilities of the parameters are given by areas contained within specific sum of squares contours. According to Box, Hunter and Hunter (1978) these areas can be calculated as follows:

For a 1-α joint confidence region of n^* and G^* the area is bounded by a sum of squares contour, S, such that:

$$S = S_R\left[1+\frac{p}{n-p}F_\alpha(p,n-p)\right] \qquad 6.4$$

where: S_R = The least sum of squares.
n = Number of data points.
p = Number of parameters.
$F_\alpha(p,n-p)$ = Significance point of the F distribution with p and n-p degrees of freedom.
α = 0.1 for a 90% confidence level.

The shaded area in figure 6.13 enclosed within the S contour supplies the 90% confidence region. The oblique orientation of the contours implies that the two values n^* and G^* are negatively correlated.

The 90% confidence region implies that if an experiment is repeated many times and a region calculated as described above, then 90% of the calculated regions will include the true parameter point and 10% will exclude it. From figure 6.13 it is noted that the 90% confidence interval stretches over large changes in n^* and G^*. This implies that for a 90% confidence region the calculated values for n^* and G^* can vary over large ranges of values, and not very accurate values for n^* an G^* can be obtained. This is understandable if it is remembered that these two values are calculated from that part of the population distribution that approaches the population density axis asymptotically.

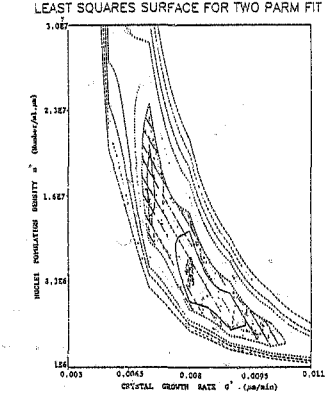

Figure 6.13 An example of a joint confidence region for the two parameter growth rate model to show the 90% confidence region for the two parameters n^* and G^*. Data from Run 17. (r=67.5min, M_c=41g/l and S=37.5g/l.)

6.7 Major nucleation processes apparent in the present system

In section 4.1 a brief description of the different nucleation mechanisms that can occur in a crystallization system was presented. Reasons are presented here to support the view that the only nucleation process occurring in this present system, is contact secondary nucleation. Each of the three types of nucleation is now discussed in the light of the experimental evidence.

6.7.1 Homogeneous nucleation

Homogeneous nucleation occurs when nuclei are formed solely because of the supersaturation driving force. In class I systems this kind of nucleation is rarely observed because it is basically a low yield system. In fact several investigators such as Randolph and Larson (1971) support the view that homogeneous nucleation is rarely observed in any kind of industrial crystallizers.

To verify the assumption that no homogeneous nucleation occurred in the tungstic acid-water system under investigation, two experiments with identical operating conditions were performed. In one of the experiments no seed crystals were added at the beginning of the run. The experiments were run for a sufficient time to verify the fact that with no seed crystals in the crystallizer absolutely nothing happened. The experimental results were that no crystals were formed in the experiment without seed crystals, while the usual crystallization of tungstic acid crystals was observed in the other crystallizer with the seed crystals present. The experimental data representing these two runs are presented in Appendix N.

Thus the assumption that homogeneous nucleation does not occur is justified.

6.7.2 Heterogeneous nucleation

This type of nucleation only occurs if foreign insoluble material is present in the system. Realising that the experimental apparatus described in section 5.1.2 was such that dust, etc. could well have entered the system, this type of nucleation could have possibly played a part in the crystallization of tungstic acid.

This possibility was eliminated after performing the experiments mentioned above in section 6.7.1, as both the experiments could have contained some form of foreign material, yet only the experiment containing seed crystals resulted in the crystallization of tungstic acid crystals taking place.

6.7.3 Secondary nucleation

A description of the three types of secondary nucleation that can take place in a crystallizing system is presented in section 4.1. A thorough explanation is also presented to support the view that only one of the three possible types, collision breeding, is important.

In the present system under consideration, this view is supported although a study of the electron micrograph photographs of the crystals shown in figures 6.8 and 6.9 suggests that the relatively larger crystals tend to be rounded. This might indicate that attrition of the crystals takes place which can cause direct birth into the measured size range. The likeliness that attrition does take place is low if the discussion in section 6.4.2 is assumed to be correct. It was mentioned there that the present tungstic acid system is a class I type system with smooth crystal-solution interfaces. According to Garside and Davey (1980) another explanation for the rounded crystals can be presented. There is a possibility of local plastic deformation distorting the crystal lattice so as to increase locally the solubility and produce rounded crystals. According to Randolph (1980) the appearance that crystals tend to get rounded as the crystal size increases is also an indication that size-dependent crystal growth rates are apparent.

Although insufficient experimental evidence exists to distinguish between the three types of secondary nucleation, the following evidence can be presented to confirm that secondary nucleation is in fact the major nucleating mechanism occurring in the present system:

a) In section 6.4.3 it is confirmed that the primary crystal growth mechanism consists of surface integration kinetics. This implies that a surface zone of partially oriented solute aggregates develops which, according to Powers (1963), is precisely what is needed for collision breeding.

b)In sections 6.9.1 and 6.9.2 it is shown that the nucleation rate increases with an increase in either stirrer speed or crystal suspension density. This is further evidence that secondary nucleation is the major nucleation mechanism apparent in this system, because an increase in the amount of collisions result in an increase in the amount of nuclei produced. This is what was predicted for contact secondary nucleation.

6.8 Behaviour of the crystal growth rate, G^*, with varying crystallization conditions

It was shown in the previous sections of this chapter that size dependent growth of the crystals occurs. In order to compare the different experiments, a crystal growth rate at a constant crystal size had to be calculated for each experiment. For the sake of the following discussions the growth rate of the nuclei sized crystals was used as a standard value to compare the different experimental results with.

6.8.1 Effect of different nuclei population densities on the crystal growth rate G^*

From figure 6.14 it can be seen that the crystal growth rate increases with a decrease in nuclei population density. This phenomenon can be explained if it is considered that the present system is a class I

crystallizing system. That is, the crystallization driving force is solely because of the evaporation of the solvent while the supersaturation stays constant all the time.

Hence, an increase in the amount of nuclei present in the system will have the effect that the available driving force will be spread amongst a larger number of crystals with the result that the growth rate of the individual crystals decreases. The overall growth rate will stay constant however.

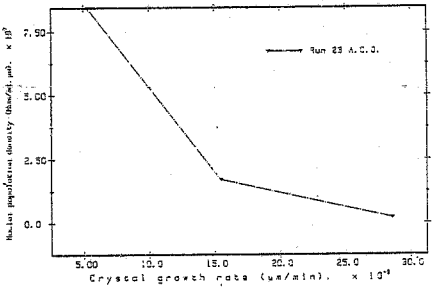

Figure 6.14 Plot of nuclei population density versus crystal growth rate of the nuclei sized crystals. The experimental conditions for these runs are presented in Appendix C.

Run 23A: n°=8.4E7 number/ml.μm G°=5.3E-3 μm/min
Run 23C: n°=1.7E7 number/ml.μm G°=1.6E-2 μm/min
Run 23D: n°=1.9E6 number/ml.μm G°=2.9E-2 μm.min

6.8.2 Effect of varying stirrer speeds on crystal growth rate G°

From figure 6.15 it is noted that an increase in stirrer speed results in a decrease in crystal growth rate. In section 6.9.1 it is shown that an increase in stirrer speed results in an increase in the nuclei population density. So, the observation that crystal growth rate increases with a decrease in stirrer speed is in agreement with what was said in the above section 6.8.1 concerning the interdependence of nucleation rate and growth rate.

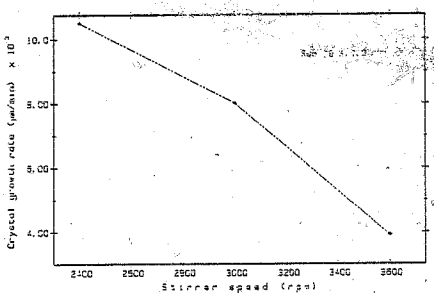

Figure 6.15 Plot of crystal growth rate of the nuclei sized crystals versus the stirrer speed in the crystallizer. The experimental conditions for these runs are presented in Appendix G.

Run 22A: G°=1.05E-2 μm/min Stirrer setting:2400 rpm
Run 22C: G°=8.00E-3 μm/min Stirrer setting:3000 rpm
Run 22D: G°=3.91E-3 μm/min Stirrer setting:3600 rpm

6.8.3 Effect of varying supersaturation on the crystal growth rate G^*

The supersaturation of a solution usually indicates the difference between the actual solution concentration of a species and the solution equilibrium concentration of that species. In the present tungstic acid system the solution equilibrium concentration of tungstic acid in water is zero because tungstic acid is completely insoluble in hot or cold water (Perry and Chilton, 1972). For the sake of this dissertation supersaturation of a tungstic acid solution will thus indicate the actual solution concentration of tungsten.

It can be observed on figure 6.16 that at high crystal suspension densities the crystal growth rates decrease with an increase in supersaturation.

It can also be observed on figure 6.16 that at low crystal suspension densities crystal growth rates increase with an increase in supersaturation.

The following explanation is possible: At high suspension density (i.e. M_t) values the nucleation mechanism is more dominant than the growth mechanism, and with an increase in supersaturation the secondary nucleation rate increases. More nuclei are thus produced, and the growth rate decreases as discussed in section 6.8.1.

At low M_t values, the growth mechanism is more dominant than the nucleation mechanism (because of the linear relationship between the nucleation rate and M_t, the nucleation rate is low if M_t is low) with the result that the amount of new nuclei produced is small and an increase in supersaturation causes an increase in the crystal growth rate.

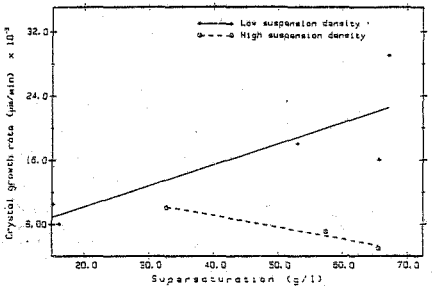

Figure 6.16 Plot of crystal growth rate of the nuclei sized crystals versus the supersaturation of the tungstic acid solution. The experimental conditions for these runs are presented in Appendix G.

High suspension density:

Run 19: G^*=1.0E-2 μm/min	S=32.7 g/l
Run 17: G^*=7.0E-3 μm/min	S=57.5 g/l
Run 18: G^*=4.9E-3 μm/min	S=65.7 g/l

Low suspension density:

Run 23B: G^*=1.8E-2 μm/min	S=53.0 g/l
Run 23C: G^*=1.6E-2 μm/min	S=65.7 g/l
Run 23D: G^*=2.9E-2 μm/min	S=67.3 g/l
Run 22A: G^*=1.05E-2 μm/min	S=15.1 g/l
Run 22C: G^*=8.0E-3 μm/min	S=16.1 g/l

6.9 Behaviour of the crystal nucleation rate with varying crystallization conditions

All the data used for the discussion of this and the previous section are summarised in Appendix I.

6.9.1 Effect of varying stirrer speeds on the nucleation rate

From figure 6.17 it can be seen that an increase in stirrer speed results in an increase in the nucleation rate. This is exactly what should happen if contact secondary nucleation dominates the system.

An increase in stirrer speed results in a larger amount of crystal-crystal and crystal-noncrystal collisions. The collisions become more intense as well. Because the collisions cause the nuclei to form, it is obvious that more nuclei and hence a larger nucleation rate, should be formed with an increase in stirrer speed.

It was also observed in figure 6.17 that when the crystal suspension density was very low the nucleation rate stayed approximately constant while the stirrer speed was varied between two certain regions. When the stirrer speed was increased even more, the usual trend of an increasing nucleation rate was observed. This phenomenon can be explained once again if secondary nucleation is considered: With a very low crystal suspension density a small increase in stirrer speed will not increase the number of collisions so drastically and the nucleation rate will stay approximately constant. If the stirrer speed increases much more the increase in the number of collisions will become significant and hence the nucleation rate will increase.

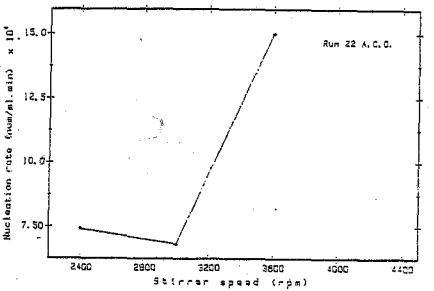

Figure 6.17 Plot of nucleation rate versus the stirrer speed in the crystallizer for various runs when the crystal suspension density is low. The experimental conditions for these runs are presented in Appendix G.
Run 22A: B°=7.4E4 number/ml.min Stirrer setting:2400 rpm
Run 22C: B°=6.8E4 number/ml.min Stirrer setting:3000 rpm
Run 22D: B°=1.5E5 number/ml.min Stirrer setting:3600 rpm

6.9.2 Effect of different crystal suspension densities on the nucleation rate

In section 6.10 it is shown that a linear relationship exists between nucleation rate and crystal suspension density for this specific system. Once again the number of collisions plays a part and hence leads to contact secondary nucleation. The same explanations as in the previous sections hold.

6.9.3 Effect of varying supersaturations on the nucleation rate

From figure 6.18 it can be noted that at a high crystal supension density the nucleation rate increases with an increase in supersaturation. At a low crystal suspension density the supersaturation has no effect on the nucleation rate.

The following explanation is possible: At high suspension densities the nucleation mechanism is more dominant than the growth mechanism because many crystal-crystal collisions take place which cause the nucleation rate to be very high. An increase in supersaturation will thus only cause the nucleation rate to increase.

At low suspension density values, the growth mechanism is more dominant than the nucleation mechanism (because of the linear relationship between the nucleation rate and M_T, the nucleation rate is low if M_T is low) with the result that the amount of new nuclei produced is small and an increase in supersaturation causes an increase in the crystal growth rate.

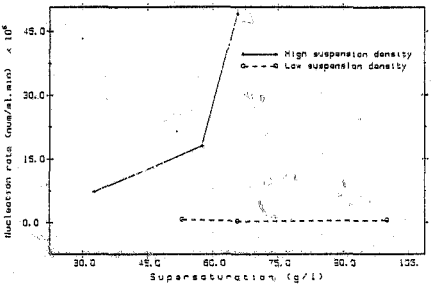

Figure 6.18 Plot of nucleation rate versus supersaturation of the tungstic acid solution in the MSMPR crystallizer. The experimental conditions for these runs are presented in Appendix G.

High suspension density:

Run 19: B^0=7.2E6 number/ml.min S=32.7 g/l

Run 17: B^0=1.8E7 number/ml.min S=57.5 g/l

Run 18: B^0=4.9E7 number/ml.min S=65.7 g/l

Low suspension density:

Run 23A: B^0=4.5E5 number/ml.min S=100.1 g/l

Run 23B: B^0=6.2E5 number/ml.min S=53.0 g/l

Run 23C: B^0=2.6E5 number/ml.min S=65.7 g/l

6.10 Empirical expressions for the nucleation and growth kinetics

In section 4.1 a discussion was presented which showed that if secondary nucleation is the dominant nucleation mechanism in the crystalliser, the following empirical nucleation expression could be used:

$$B^{\circ} = K_M S^i M_T^j \qquad 6.5$$

The empirical expression generally used to describe the crystal growth rate is a simple function of supersaturation:

$$G = G(S) \qquad 6.6$$

In the present tungstic acid system, however, the growth rate is size dependent and the following empirical growth rate expression was presented in section 6.5:

$$G = G^{\circ} (1+\gamma L)^{0.58} \qquad 6.2$$

Where $\gamma = 1/G^{\circ}\tau$

G° = Growth rate of the nuclei sized crystals.

In order to use the above expression G° must be known. It is assumed that G° is a simple function of supersaturation:

$$G^{\circ} = K_G S \qquad 6.7$$

Combining equations 6.5 and 6.7, and eliminating the supersaturation gives the following expression:

$$B^{\circ} = k_R M_T^{j} G^{\circ i} \qquad 6.8$$

For a system where the suspension density is linearly related to the nucleation rate the value of j equals 1. It can be noted from figure 6.19 that because the curves are parallel this is the case in the present system since the same CSD arises when two different suspension densities are used.

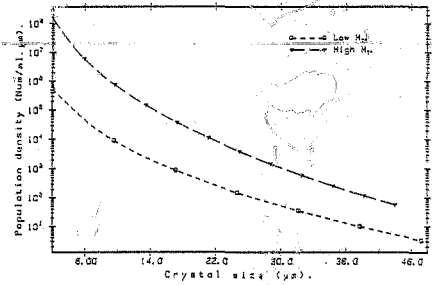

Figure 6.19 Semilog plot of population density versus crystal size for two different suspension densities. The experimental conditions for these two runs are presented in Appendix G.
Run 19:
M_T=52.6 g/l n°=7.2E8 number/ml.μm G°=1.0E-2 μm/min

Run 22D:
M_T=9.3 g/l n°=3 9E6 number/ml.μm G°=3.9E-3 μm/min

With the value of j known, the value of i can be obtained. This is done by plotting log B° versus log G° for different experiments, all with the same suspension density. This curve should be a straight line with a slope equal to i. This has been done in figure 6.20 and the resulting value of i has been obtained as approximately -2.9.

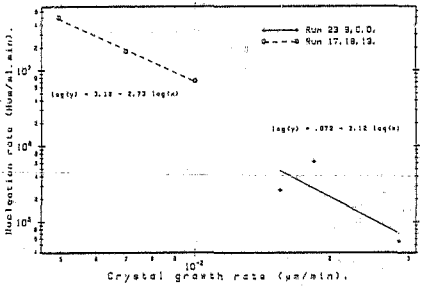

Figure 6.20 Log log plot of nucleation rate versus crystal growth rate of the nuclei sized crystals in order to calculate the value of the kinetic order i. The experimental conditions for these runs are presented in Appendix G.
Run 23B: B°=6.2E5 number/ml.min G°=1.8E-2 μm/min
Run 23C: B°=2.6E5 number/ml.min G°=1.6E-2 μm/min
Run 23D: B°=5.5E4 number/ml.min G°=2.9E-2 μm/min
Run 17: B°=1.8E7 number/ml.min G°=7.0E-3 μm/min
Run 18: B°=4.9E7 number/ml.min G°=4.9E-3 μm/min
Run 19: B°=7.2E6 number/ml.min G°=1.0E-2 μm/min

7. CONCLUSIONS AND RECOMMENDATIONS

The crystallization of tungstic acid from an electrolytically produced supersaturated solution is a new concept that has not enjoyed much attention in the literature. The various aims of the research were thus to:

a) Investigate the possibility of experimentally producing tungstic acid crystalline material from an electrolytically produced supersaturated tungstic acid solution.

b) Study the nucleation and growth kinetics of this system.

The possibility of producing tungstic acid crystals was confirmed when yellow tungstic acid material was produced in an evaporative MSMPR crystallizer after seeding the crystallizing solution. The material had an X-ray diffraction pattern which confirmed that the monohydrate form, $WO_3.H_2O$, was formed and that the material was crystalline. During the crystallization experiments it was also confirmed that the present crystallizing system is a class I type crystallizing system.

After accomplishing the crystallization of tungstic acid crystals, various runs were conducted to study the nucleation and growth kinetics of the system. The literature suggested that there are basically three nucleation mechanisms that can play a part in a crystallization system. It also suggested that most MSMPR crystallizing systems behave ideally. It was found experimentally that contact secondary nucleation was the main nucleation mechanism in the crystallization of tungstic acid, and that the MSMPR crystallizer did not behave ideally. The non-ideal behaviour arose because of the size dependant crystal growth mechanism which occurred in the system. This size dependence of the growth rates could be explained if surface integration kinetics were assumed to be the dominating mechanism for

crystal growth in the system. Experimental evidence was found to support this assumption.

A size dependent growth rate model was proposed and tested and used to incorporate this size dependence of the crystal growth rates in the population balance equation. The model used, and the resulting population balance equation which was fitted to the experimental data, were as follows:

$$G(L) = G^{\circ}(1+\gamma L)^{0.58} \qquad L \geq 0 \qquad 7.1$$

Where: G(L) = Size dependent crystal growth rate.
G° = Crystal growth rate of the nuclei sized crystals.
$\gamma = 1/(G^{\circ}\tau)$
L = Characteristic crystal dimension.

$$n(L) = K_3 n^{\circ}(1+\gamma L)^{-0.58}\exp\left[-\frac{(1+\gamma L)^{0.42}}{0.42}\right] \qquad 7.2$$

Where: n(L) = Population density as a function of crystal size.
K_3 = exp(1/0.42)
n° = Population density of the nuclei sized crystals.

A confidence interval was calculated to determine the accuracy of the two calculated values G° and n° and it was found that these two values could vary over a wide range.

Experiments were then conducted to investigate the behaviour of the crystal growth and nucleation kinetics with varying crystallization conditions. It was found that:

1). Crystal growth rates decreased with increase in nuclei population density.

2) Crystal growth rates decreased with increasing stirrer speeds.

3) For a high suspension density: Crystal growth rates decreased with increase in supersaturation.

4) For a low suspension density: Growth rates increased with increase in supersaturation.

5) Nucleation rates increased with increase in stirrer speed.

6) A linear relationship existed between nucleation rate and crystal suspension density for this specific system.

7) For a high suspension density: Nucleation rates increased with increase in supersaturation.

8) For a low suspension density: Nucleation rates were not affected by changes in supersaturation.

Finally, the following empirical expressions were derived for the nucleation and growth rates:

For the secondary nucleation rate:

$$B^{\circ} = K_M S^i M_t^j \qquad 7.3$$

Where: B° = Secondary nucleation rate.
K_M = Proportionality constant.
S = Supersaturation.
M_t = Suspension density.
i and j are kinetic orders.

For the size dependent crystal growth rates:

$$G = G^{\circ}(1+\gamma L)^{0.58} \qquad 7.4$$

Where: G = Size dependent crystal growth rate.
G° = Growth rate of the nuclei sized crystals.
$\gamma = 1/G^{\circ}\tau$
L = Characteristic dimension of the crystals.

If it was assumed that G° was a simple function of supersaturation, equation 7.3 could then be rewritten as:

$$B^{\circ} = K_R M_t^j G^{\circ i} \qquad 7.5$$

From the experimental results it was found that j=1. This meant that for the tungstic acid crystallization system, the suspension density was linearly related to the nucleation rate. With the value of j known, the value of i was obtained. The resulting value of i was found to be approximately -2.9. This indicated that an inverse relationship existed between the nucleation rate and the growth rate of the nuclei sized crystals.

Recommendations for further work

1) No conclusive experimental evidence was obtained to prove that growth rate dispersion did not play a part in the crystallization of the tungstic acid crystals. This is an important phenomenon that must be further investigated.

2) It was concluded that secondary nucleation is the main nucleation mechanism in the tungstic acid crystallization process. The experimental evidence demonstrating that heterogeneous nucleation did not play a part in the system is not very reliable, and some further research into this phenomenon should be done. There was also not enough experimental evidence to distinguish between the three secondary nucleation mechanisms.

3) Another important factor which must be determined is whether the tungstic acid crystals produced can be calcined directly to produce tungsten oxide, an intermediate in the production of tungsten. If this is possible the APT intermediate in the process can be eliminated which will mean additional saving in the process.

4) Another important assessment that must be made is whether the CSD of the crystals can be controlled to a certain accuracy with the help of the kinetics established in this dissertation, and whether the overall size of the crystals can be enlarged by using several crystallizers in series.

8. REFERENCES

Abegg, C.F., Stevens, J.D. and Larson, M.A. (1968) *"Crystal Size Distributions in Continuous Crystallizers when Growth Rate is Size Dependent"*, AIChE Journal, vol. 14, no. 1, pp. 118-122.

Bennema, P. and Gilmer, G.H. (1973) "Kinetics of Crystal Growth" in Garside, J., Phillips, V.R. and Shah, M.B. (1976) *"On Size-Dependent Crystal Growth"*, Ind. Eng. Chem., Fundam., vol. 15, no. 3, pp. 230-233.

Bennet, R.C. (1962) *"Product size distribution in commercial crystallizers"*, Chem. Eng. Progr., vol. 58, no. 9, pp. 76.

Box, G.E.P., Hunter, W.G. and Hunter, J.S. (1978) *"Statistics for Experimenters"*, John Wiley and Sons, New York.

Branson, S.H. (1960), Brit. Chem. Eng., vol. 5, p.838. in Garside, J. (1980) *"Advances in the Characterisation of Crystal Growth"*, AIChE Symposium Series, vol. 80, no. 240, pp. 23-38.

Burton, W.K., Cabrera, N. and Frank, F.C. (1951) in Garside, J., Phillips, V.R. and Shah, M.B. (1976) *"On Size-Dependent Crystal Growth"*, Ind. Eng. Chem., Fundam., vol. 15, no. 3, pp. 230-233.

Canning, T.F. and Randolph, A.D. (1980), AIChE Journal, vol. 13, no. 5 in Garside, J. (1980) *"Advances in the Characterisation of Crystal Growth"*, AIChE Symposium Series, vol. 80, no. 240, pp. 23-38.

Canterford, J.H. and Colton, R. (1968) "*Halides of the Second and Third Row Transition Metals*", John Wiley and Sons, New York.

Cayey, N.W. and Estrin, J. (1967) "*Secondary Nucleation in Agitated, Magnesium Sulfate Solutions*", Ind. Eng. Chem. Fundamentals, vol. 6.

Clontz, N.A. and McCabe, L.W. (1971) "*Concacr Nucleation of Magnesium Sulfate Heptahydrate*", Chem. Eng. Progr. Symp. Ser., vol. 67, no. 6.

Comey, A.M. and Hahn, D.A. (1921) "*A Dictionary of Chemical Solubilities - Inorganic*", The MacMillan Company, New York.

Desai, R.M., Rachow, J.W. and Timm, D.C. (1974) "*Collision Breeding: A Function of Crystal Moments and Degree of Mixing*", AIChE Journal, vol. 20, no. 1, pp. 43-50.

de Jong, E.J. (1984) "*Development of Crystallizers*", International Chemical Engineering, vol. 24, no. 3, pp. 419-431.

Fourie, A.J. (1983) "*Pilot Plant Filtration Testwork Performed on a 1 m^2 Belt Filter*", Council for Mineral Technology report no. 18069.

Garside, J., Mullin, J.W. and Das, S.N. (1974) in Garside, J., Phillips, V.R. and Shah, M.B. (1976) "*On Size-Dependent Crystal Growth*", Ind. Eng. Chem., Fundam., vol. 15, no. 3, pp. 230-233.

Garside, J., Janssen-van Rosmalen, R. and Bennema, P. (1975) in Garside, J., Phillips, V.R. and Shah, M.B. (1976) "*On Size-Dependent Crystal Growth*", Ind. Eng. Chem., Fundam., vol. 15, no. 3, pp. 230-233.

Garside, J., Phillips, V.R. and Shah, M.B. (1976) "*On Size-Dependent Crystal Growth*", Ind. Eng. Chem., Fundam., vol. 15, no. 3, pp. 230-233.

Garside, J. and Jancic, S.J. (1976) " *Growth and Dissolution of Potash Alum Crystals in the Subsieve Size Range*", AIChE Journal, vol. 22, no. 5, pp. 887-894.

Garside, J. (1980) "*Advances in the Characterisation of Crystal Growth*", AIChE Symposium Series, vol. 80, no. 240, pp. 23-38.

Garside, J. and Davey, R.J. (1980) "*Secondary Contact Nucleation: Kinetics, Growth and Scale-up*", Chem. Eng. Commun., vol. 4, pp. 393-424.

Janse, A.H. and de Jong, E.J. pp. 145 in Mullin, J.W. (1976) "*Industrial Crystallization*", Plenum Press, New York.

Johnson, R.T., Rousseau, R.W. and McCabe, W.L. (1970) in Youngquist, G.R. and Randolph, A.D. (1972) "*Secondary Nucleation in a Class II System: Ammonium Sulfate-Water*", AIChE Journal, vol. 18, no. 2, pp. 421-429.

Lal, D.P., Mason, R.E.A. and Strickland-Constable, R.F. (1969) in Youngquist, G.R. and Randolph, A.D. (1972) "*Secondary Nucleation in a Class II System: Ammonium Sulfate-Water*", AIChE Journal, vol. 18, no. 2, pp. 421-429.

Larson, M.A., Timm, D.C. and Wolff, F.R. (1968) "*Effect of Suspension Density on Crystal Size Distribution*", AIChE Journal, vol. 14, no. 3, pp. 448-451.

Larson, M.A. (1980) "*Advances in the Characterization of Crystal Nucleation*", AIChE Symposium Series, vol. 80, no. 240, pp. 39-44

Larson, M.A. (1981) "*Secondary Nucleation: An Analysis*", Chem. Eng. Commun., vol. 12, pp 161-169.

Mason, R.E.A. and Strickland-Constable, R.F. (1966) in Youngquist, G.R. and Randolph, A.D. (1972) "*Secondary Nucleation in a Class II System: Ammonium Sulfate-Water*", AIChE Journal, vol. 18, no. 2, pp. 421-429.

Mersmann, A. (1984) "*Design and Scale-up of Crystallizers*", International Chemical Engineering, vol. 24, no. 3, pp. 401-418.

Moore, W.J. (1962) "*Physical Chemistry*", Prentice-Hall Inc., New York.

McCabe, W.L. and Stevens, R.P. (1951) in Abegg, C.F., Stevens, J.D. and Larson, M.A. (1968) "*Crystal Size Distributions in Continuous Crystallizers when Growth Rate is Size Dependent*", AIChE Journal, vol. 14, no. 1, pp. 118-122.

McCabe, W.I and Smith, J.C. (1976) *"Unit operations of chemical engineering"*, McGraw-Hill Book Co., New York.

Perry and Chilton (1972) *"Chemical Engineers Handbook"*, 5 th ed., McGraw-Hill Book Co., New York.

Phillips, V.R. and Epstein, N. (1974) in Garside, J., Phillips, V.R. and Shah, M.B. (1976) *"On Size-Dependent Crystal Growth"*, Ind. Eng. Chem., Fundam., vol. 15, no. 3, pp. 230-233.

Pourbaix, M. (1974) *"Atlas of Electrochemical Equilibria in Aqueous Solutions"*, National Association of Corrosion Engineers, 2 nd Ed., pp. 280-284.

Powers, H.E.C. (1963) *"Nucleation and Early Crystal Growth"*, Ind. Chem., vol. 39, pp. 351.

Ramanarayanan, K.A., Athreya, K. and Larson, M.A. (1980) *"Statistical-Mathematical Modelling of CSD in Continuous and Batch Crystallizers"*, AIChE Symposium Series, vol. 80, no. 240, pp. 76-88.

Randolph, A.D. and Larson, M.A. (1962) *"Transient and Steady State Size Distributions in Continuous Mixed Suspension Crystallizers"* AIChE Journal, vol. 8, no. 5, pp. 639-645.

Randolph, A.D. (1965) *"The Mixed Suspension, Mixed Product Removal Crystallizer as a Concept in Crystallizer Design"*, AIChE Journal, vol. 11, no. 3, pp. 424-430.

Randolph, A.D. (1969) "*Effect of Crystal Breakage on Crystal Size Distribution in a Mixed Suspension Crystallizer*", I.& E.C. Fundamentals, vol. 8, no. 1, pp. 58-63.

Randolph, A.D. and Larson, M.A. (1971) "*Theory of Particulate Processes*", Academic Press, New York.

Randolph, A.D. and Cise, M.D. (1972) "*Nucleation Kinetics of the Potassium Sulfate-Water System*", AIChE Journal, vol. 18, no. 4, pp. 798-867.

Randolph, A.D. (1980) "*CSD Dynamics, Scability, and Control*", AIChE Symposium Series, vol. 76, no. 193, pp. 1-5.

Reed-Hill, R.E. (1968) "*Physical Metallurgy Principles*", D. Van NOSTRAND Company, INC., Canada.

Rosen, H.N. and Hulburt, H.M. (1971) "*Growth Rate of Potassium Sulfate in a Fluidized-Bed Crystallizer*", Chem. Eng. Progr. Ser., vol. 67.

Rumford, F. and Bain, J. (1960) in Abegg, C.F., Stevens, J.D. and Larson, M.A. (1968) "*Crystal Size Distributions in Continuous Crystallizers when Growth Rate is Size Dependent*", AIChE Journal, vol. 14, no. 1, pp. 118-122.

Shor, S.M. and Larson, M.A. (1971) "*Effect of Additives on Crystallization Kinetics*", Chem. Eng. Progr. Symp. Ser., vol. 67.

Stephen, W.H. and Wang, C.T. (1981) "*Tungsten Sources, Metallurgy Properties, and Applications*", Plenum Press, New York.

Strickland-Constable, R.F. (1972) "*Breeding of crystal nuclei. Review of the subject*", AIChE Symp. Ser., vol. 68, no. 1.

Timm, D.C. and Larson, M.A. (1968) "*Effect of Nucleation Kinetics on the Dynamic Behaviour of a Continuous Crystalliser*", AIChE Journal, vol. 14, no. 3, pp. 452-457.

Topkaya, Y.A. and Eric, H. (1982) "*Laboratory Testing of Uludag Scheelite Concentrate for the Production of Ammonium Paratungstate*", Middle East Technical University, Report no. B4/1.

Verbaan, B., Greenslade, D.N. and Wade, W.G. (1984) "*The Selective Electrolytic Removal of Sodium from Sodium Carbonate and Sodium Tungstate using a Cation Selective Membrane*", Final year project report.

Verbaan, B. (1985) "*Removal of Sodium Ions from Alkaline Aqueous Solutions by Means of an Electrolytic Membrane Process*", South African Patent no. 85/1119.

Verbaan, B. and Brown, G.A. (1986) "*The Membrane Electrolysis of Aqueous Solutions Containing Sodium Carbonate and/or Sodium Tungstate*", Paper presented at the 13th CMMI congress-Metallurgy, vol. 4, pp. 197-203.

Weast, R.C. (1976) "*Handbook of Chemistry and Physics*", CRC Press, Cleveland, Ohio.

Yeager, H.L. and Steck, A. (1981) "*Cation and Water Diffusion in Nafion Exchange Membrane: Influence of Polymer Structure:*", Journal of Electrochem. Soc., vol. 128, no. 9, pp. 1880-1884.

Youngquist, G.R. and Randolph, A.D. (1972) "*Secondary Nucleation in a class II System: Ammonium Sulfate-Water*", AIChE Journal, vol. 18, no. 2, pp. 421-429.

APPENDIX A

Purification of the sodium tungstate leach solution from impurities such as silica, phosphorous, arsenic and molybdenum.

A.1 The preliminary silica-removal step

According to Topkaya and Eric (1982) sodium tungstate leach solutions are generally contaminated with silica, phosphorous, arsenic, and molybdenum, which are usually present in the raw material. These must be reduced to acceptable levels before further processing of the leach solution. If the silica level is above 2 to 5 g/l a preliminary silica-removal step is required.

The first step is the addition of alum ($Al_2(SO_4)_3.18H_2O$) and magnesium sulphate ($MgSO_4.7H_2O$) to the leach solution before the filtration of this solution to remove the unreacted gangue. The alum and magnesium sulphate are added in quantities of between 0.03 and 0.08 kg per kilogram of WO_3, respectively. The solution is stirred for 1 hour at 70 to 80 °C and then filtered. This procedure decreases the silica level in the solution to 2 g/l or below. After filtering, the solution is treated once more with alum and magnesium sulphate to decrease the silica level to the range 0.03 to 0.06 g/l. Both purification steps are conducted at a pH value between 9 and 9.5. Filtering after the secondary step must be performed with more care, possibly by the use of a filter aid such as cellulose. The tungsten loss during these processes is about 1 % of the total value.

The pertinent precipitation reactions are as follows:

$$2Na_2SiO_3 + Al_2(SO_4)_3 + nH_2O + 2Na_2CO_3 \rightleftharpoons Na_2O.Al_2O_3.2SiO_2.nH_2O + 2CO_2 + 3Na_2SO_4 \quad A.1$$

and

$$Na_2SiO_3 + 2MgSO_4 + Na_2CO_3 \rightleftharpoons 2MgO.SiO_2 + 2Na_2SO_4 + CO_2 \quad A.2$$

A mixture of alum and magnesium sulphate will also remove phosphorous from the solution.

A.2 The preliminary molybdenum-removal step

According to Topkaya and Eric (1982) molybdenum removal is performed by the precipitation as molybdenum trisulphide.

The first step is the formation of thiomolybdate ions by the reaction:

$$MoO_4^{2-} + 4S^{2-} + 4H_2O \rightleftharpoons MoS_4^{2-} + 8OH^- \quad A.3$$

The sulphide is added as sodium sulphide or sodium hydrogen sulphide at a pH>10. Conversion of the thiomolybdate is complete in 1-2 hours at 80-85°C. The amount of sulphide required for acceptable molybdenum removal depends upon the ratio of Mo:W and upon the concentration of tungsten. Usually, three times the amount of sulphide required stoichiometrically is sufficient for a Mo:W ratio of 0.01 to 0.02. A decreasing Mo:W ratio requires an increasing sulphide addition.

Following the formation of the thiomolybdate complex, molybdenum is precipitated as MoS_3 by acidifying to pH 2.5-3 while stirring the solution at 80°c over a period of 2-9 hours. The pertinent reaction is:

$$MoS_4^{2-} + 2H_3O^+ \rightleftharpoons MoS_3 + H_2S + 2H_2O \qquad A.4$$

During this process, precipitation of other sulphide-forming elements, especially antimony, arsenic, bismuth, copper and lead are also possible.

The molybdenum trisulphide and other sulphida precipitates, if present, are removed by filtration. The cake is then washed with slightly acidic water to minimize tungsten loss. The molybdenum removal step reduces the molybdenum level to less than 10 mg/l. Tungsten losses in this step are about 1 % of the throughput. During the removal of silica and molybdenum, phosphorus and arsenic are reduced to less than 20mg/l and 3mg/l, respectively. No special purification steps for these two contaminants are therefore necessary.

APPENDIX B

Electrochemistry in the two electrolytic membrane processes.

According to Verbaan, Greenslade and Wade (1984) there are two distinct regions present in the electrolytic conversion of sodium carbonate and tungstic acid if both of these solutions are present in the anode solution. Initially, the sodium flux is constant at a membrane efficiency of 98 %, a value that is characteristic of the removal of sodium from sodium carbonate. At a certain catholyte concentration of sodium ions the flux drops very rapidly to a constant value corresponding to a membrane efficiency of approximately 80 %. The catholyte concentration where this drop in membrane efficiency occurs is at the point where nearly all the sodium carbonate has been converted to carbonic acid and sodium removal is from the sodium tungstate alone.

Because of this observation the two electrolytic membrane processes, i.e. the electrolytic removal of sodium from sodium carbonate and the electrolytic removal of sodium from sodium tungstate, will be treated as two independent processes which take place.

B.1 Electrolytic removal of sodium from sodium carbonate

A schematic representation of the chemistry involved is shown in figure B.1.

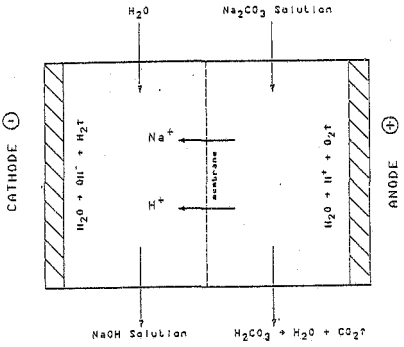

Figure B.1 Schematic representation of the electrolytic removal of sodium ions from sodium carbonate

In both the anode and cathode compartments, the dissociation of water occurs. Oxygen is liberated at the anode and hydrogen at the cathode:

Anode: $H_2O \rightleftharpoons 2H^+ + 2e^- + 1/2\ O_2\uparrow$ B.1

Cathode: $2H_2O + 2e^- \rightleftharpoons 2OH^- + H_2\uparrow$ B.2

The cation selective membrane which separates the anode from the cathode compartment ideally only allows movement of positive ions through it. In this case the anolyte is a sodium carbonate solution, with the result that the only cations present are the sodium ions and protons arising from the dissociation of water at the anode.

As these cations migrate through the membrane they combine with the hydroxide ions in the cathode to produce caustic soda and water respectively as follows:

$$H^+ + OH^- \rightarrow H_2O \qquad B.3$$

$$Na^+ + OH^- \rightarrow NaOH \qquad B.4$$

As the anolyte loses sodium through the membrane, the carbonate ions will take up protons to form carbonic acid:

$$Na_2CO_3 \rightarrow NaCO_3^- + Na^+ \qquad B.5$$

$$NaCO_3^- + H^+ \rightarrow NaHCO_3 \qquad B.6$$

$$NaHCO_3 \rightarrow HCO_3^- + Na^+ \qquad B.7$$

$$HCO_3^- + H^+ \rightarrow H_2CO_3 \qquad B.8$$

At atmospheric pressure, carbonic acid readily decomposes into carbon dioxide and water:

$$H_2CO_3 \rightarrow CO_2\uparrow + H_2O \qquad B.9$$

It is important to know that the competition of the H^+ ions with the Na^+ ions, and the backmigration of OH^- ions cause membrane inefficiency.

B.2 Electrolytic removal of sodium from sodium tungstate

A schematic representation of the chemistry involved is shown in figure B.2. Once again water is dissociated at the electrodes and because the tungstate radical does not form any positive complexes, Pourbaix (1974), the only cations that compete to move through the cation selective membrane are the protons and sodium ions.

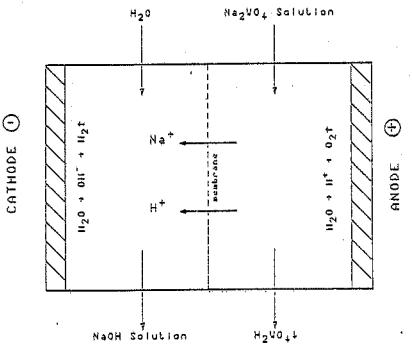

Figure B.2 Schematic representation of the electrolytic removal of sodium ions from sodium tungstate

Sodium removed from the tungstate radical will be replaced with protons from the dissociation of water at the anode to produce tungstic acid:

$$Na_2WO_4 \rightleftharpoons NaWO_4^- + Na^+ \qquad B.10$$

$$NaWO_4^- + H^+ \rightleftharpoons NaHWO_4 \qquad B.11$$

$$NaHWO_4 \rightleftharpoons Na^+ + HWO_4^- \qquad B.12$$

$$HWO_4^- + H^+ \rightleftharpoons H_2WO_4 \qquad B.13$$

Because the tungstic acid formed in the anode solution has a very high supersaturation it can be crystallized out directly using an evaporative MSMPR crystallizer.

APPENDIX C

Faraday's Law.

In both the electrolytic membrane processes outlined in Appendix B, the time needed to transport a given amount of sodium ions from the anode to the cathode compartments can be calculated using Faraday's Law (Moore, 1962) as follows:

$$t = \frac{m\ Z\ F}{M\ I\ \eta} \qquad C.1$$

Where: t = Time (s).
m = Mass of sodium ions to be transported per unit area (g/m^2).
Z = Number of charges on the sodium ion (-).
F = Faraday's constant. (96485 C/mol)
M = Atomic weight of sodium (g/mol).
I = Current density (Amp/m^2).
η = Membrane efficiency (-).

APPENDIX D

Definition of the electrolytic cell membrane efficiency.

The current supplied to the electrolytic membrane process is used to transport all the available cations from the anode across the membrane to the cathode. This means that protons which are present in the processes as a result of the dissociation of water are also transported across the cation selective membrane. This phenomenon is undesireable because it reduces the sodium flux through the membrane. To eliminate the latter effect, it is economical to choose operating conditions so as to maximise the sodium ion flux through the membrane. Another factor which may contribute towards membrane inefficiency is the possible backmigration of OH^- ions across the membrane. This effect also reduces the sodium flux through the membrane.

In order to draw comparisons between various experimental runs it is convenient to define the membrane efficiency as:

$$\eta = \frac{\text{Observed sodium flux}}{\text{Theoretical maximum flux}} * 100\ \% \qquad \text{D.1}$$

The maximum flux is the flux which will be observed if sodium ions are the only ions which move through the membrane. This is given by Faraday's law (Refer to Appendix C):

$$N = \frac{I}{F} \qquad \text{D.2}$$

Where: N = Molar flux of sodium ions (mol/s.m^2).
I = Current density (Amp/m^2).
F = Faraday's constant. (96485 C/mol)

APPENDIX E

Nature of the cation selective membranes.

Ion exchange membranes consist of a physical support upon which a polymer with highly ionisable functional groups is supported. These ionisable groups consist of fixed anions and mobile counter cations in a cation selective membrane. The result is a rugged sheet having ion selectivity and corrosion resistance, dependending on the nature of the polymer used.

The membranes are essentially impermeable to water but highly permeable to ions of opposite charge to the charge on the fixed ionised functional groups in the membrane. Ions of the same charge as the fixed ions however, are repelled and are ideally impermeable.

It has been suggested by Yeager and Stack (1981) that the membrane can be considered to consist of three structural zones;

a)Regions impermeable to ions, regardless of their charge, which consists of the polymer backbone and the physical support.

b)The active sites through which ion transport occurs. These regions are viewed as being of relatively large fractional voidage. These volumes contain a small amount of sorbed water and ion clusters.

c)A region loosely termed as the transition between the above two regions.

Ideally then, the current through a membrane will be solely due to the movement of charge-carrying species through the active sites and not due to any bulk transport through the membrane.

APPENDIX F

Derivation of the population balance equation for the ideal MSMPR crystallizer.

In a given volume the number of crystals of each size range must be conserved for the system to be in equilibrium. The crystal population balance is:

Number in by feed stream + Number in by growth = Number out by product stream + Number out by growth.

$$Q_i \bar{n}_i \Delta L \Delta t + V n_1 G_1 \Delta t = Q \bar{n} \Delta L \Delta t + V n_2 G_2 \Delta t \qquad F.1$$

Where: n_1= number crystals of size L_1 in volume V.
n_2= number crystals of size L_2 in volume V.
Δt=Time interval.
G_1=Crystal growth rate at size L_1.
G_2=Crystal growth rate at size L_2.
Q_i=Volumetric flow rate in.
Q =Volumetric flow rate out.
ΔL=Size difference, L_2-L_1.
V =Total volume of the crystal magma.
$\bar{n}$ =Average population density in size range L_1 to L_2.

Rearranging equation F.1:

$$V (G_2 n_2 - G_1 n_1) = (Q_i \bar{n}_i - Q \bar{n}) \Delta L \qquad F.2$$

As ΔL approaches zero, the average values of n become point values and equation F.2 takes the form:

$$V \frac{d(G n)}{dL} = Q_i n_i - Q n \qquad F.3$$

For an unseeded system or one with no crystals in the feed large enough to be in the size range under consideration, $n_i = 0$ and:

$$\left(\frac{V}{Q}\right) \frac{d(G n)}{dL} + n = 0 \qquad F.4$$

For the idealized crystallizer the ΔL law holds and G is not a function of size L. Also, the residence time, τ, is defined as V/Q. Then:

$$G\tau \left(dn/dL \right) + n = 0 \qquad F.5$$

Then n^o is defined as the population density of the nuclei as their size is close to zero. With this boundary condition, equation F.5 can be integrated as:

$$\int_{n^o}^{n} \frac{dn}{n} = -\int_{o}^{L} \frac{dL}{G\tau} \qquad F.6$$

$$\text{Giving: } n = n^o \exp \left(-L / G\tau \right) \qquad F.7$$

This is the fundamental population balance equation.

APPENDIX G

Raw data from the MSMPR crystallizer exhibiting the weight fraction of crystals in each size range.

The first thirteen runs are not used since various experimental problems were encountered during these runs which made these runs meaningless.

The following parameters were determined during each run:

Oilbath temperature: The temperature of the heating medium in which the MSMPR crystallizer was immersed.

Stirrer speed: The rotation speed of the stirrer which was used to keep the crystals in the MSMPR crystallizer in suspension.

Drawdown time of vessel: The mean residence time of the crystals in suspension.

Crystal suspension density: The suspension density of the crystallizer magma at steady state conditions.

Supersaturation: The supersaturation of a solution usually indicates the difference between the actual solution concentration of a species and the solution equilibrium concentration of that species. In the present tungstic acid system the solution equilibrium concentration of tungstic acid in water is zero because tungstic acid is completely insoluble in hot or cold water (Perry and Chilton, 1972). For the sake of this dissertation supersaturation of a tungstic acid solution will

thus indicate the actual solution concentration of tungsten.

Various runs were conducted, each time varying one or more of the parameter values.

Run 14.

Oilbath temperature : 160 °C

Stirrer speed : 4000 rpm

Drawdown time of vessel : 49.4 min

Crystal suspension density : 61.98 g/l

Supersaturation of tungsten: 51.14 g/l

Weight fraction of crystals %	Crystal size range from (μm)	to (μm)
1.5	54.9	33.7
6.0	33.7	23.7
16.9	23.7	17.7
28.4	17.7	13.6
18.7	13.6	10.5
7.7	10.5	8.2
5.2	8.2	6.4
6.7	6.4	5.0
5.8	5.0	3.9
1.8	3.9	3.0
0.8	3.0	2.4
0.4	2.4	1.9
0.1	1.9	1.5

Run 15.

Oilbath temperature : 160 °C

Stirrer speed : 4000 rpm

Drawdown time of vessel : 48.6 min

Crystal suspension density : 18.59 g/l

Supersaturation of tungsten: 41.15 g/l

Weight fraction of crystals %	Crystal size range from (μm)	to (μm)
0.1	54.9	33.7
2.8	33.7	23.7
11.0	23.7	17.7
23.7	17.7	13.6
26.5	13.6	10.5
15.9	10.5	8.2
5.3	8.2	6.4
3.5	6.4	5.0
6.0	5.0	3.9
3.3	3.9	3.0
1.0	3.0	2.4
0.6	2.4	1.9
0.2	1.9	1.5
0.1	1.5	1.2

Run 17.

Oilbath temperature : 140 °C

Stirrer speed : 3600 rpm

Drawdown time of vessel : 67.5 min

Crystal suspension density : 40.98 g/l

Supersaturation of tungstan: 57.45 g/l

Weight fraction of crystals %	Crystal size range from (μm)	to (μm)
0.3	118.4	54.9
1.5	54.9	33.7
3.5	33.7	23.7
11.3	23.7	17.7
21.4	17.7	13.6
22.2	13.6	10.5
20.8	10.5	8.2
8.8	8.2	6.4
4.5	6.4	5.0
5.2	5.0	3.9
0.4	3.9	3.0

Run 18.

Oilbath temperature : 140 °C

Stirrer speed : 3600 rpm

Drawdown time of vessel : 67.5 min

Crystal suspension density : 57.12 g/l

Supersaturation of tungsten: 65.7 g/l

Weight fraction of crystals %	Crystal size range from (μm)	to (μm)
0.3	54.9	33.7
3.1	33.7	23.7
14.8	23.7	17.7
17.1	17.7	13.6
9.9	13.6	10.5
6.7	10.5	8.2
10.1	8.2	6.4
10.4	6.4	5.0
5.2	5.0	3.9
4.6	3.9	3.0
6.2	3.0	2.4
5.0	2.4	1.9
2.2	1.9	1.5
1.1	1.5	1.2

Run 19.

Oilbath temperature : 140 °C

Stirrer speed : 3600 rpm

Drawdown time of vessel : 67.5 min

Crystal suspension density : 52.56 g/l

Supersaturation of tungsten: 32.73 g/l

Weight fraction of crystals %	Crystal size range from (μm)	to (μm)
0.2	54.9	33.7
5.3	33.7	23.7
33.2	23.7	17.7
39.1	17.7	13.6
5.0	13.6	10.5
0.9	10.5	8.2
11.8	8.2	6.4
3.2	6.4	5.0
0.0	5.0	3.9
0.0	3.9	3.0
0.3	3.0	2.4
0.6	2.4	1.9
0.2	1.9	1.5
0.1	1.5	1.2

Run 20.

Oilbath temperature : 140 °C

Stirrer speed : 2500 rpm

Drawdown time of vessel : 51.0 min

Crystal suspension density : 12.10 g/l

Supersaturation of tungsten: 26.78 g/l

Weight fraction of crystals %	Crystal size range from (μm)	to (μm)
0.2	33.7	23.7
2.4	23.7	17.7
11.7	17.7	13.6
26.7	13.6	10.5
26.9	10.5	8.2
13.3	8.2	6.4
8.3	6.4	5.0
7.0	5.0	3.9
1.7	3.9	3.0
0.7	3.0	2.4
0.9	2.4	1.9
0.2	1.9	1.5

Run 22 A.

Oilbath temperature : 140 °C

Stirrer speed : 2400 rpm

Drawdown time of vessel : 78.6 min

Crystal suspension density : 0.968 g/l

Supersaturation of tungsten: 15.05 g/l

Weight fraction of crystals %	Crystal size range from (µm)	to (µm)
5.2	118.4	54.9
12.9	54.9	33.7
10.2	33.7	23.7
10.3	23.7	17.7
9.5	17.7	13.6
7.8	13.6	10.5
9.0	10.5	8.2
13.6	8.2	6.4
13.6	6.4	5.0
6.1	5.0	3.9
1.5	3.9	3.0
0.3	3.0	2.4

Run 22 G.

Oilbath temperature : 140 °C

Stirrer speed : 3000 rpm

Drawdown time of vessel : 78.6 min

Crystal suspension density : 0.467 g/l

Supersaturation of tungsten: 16.14 g/l

Weight fraction of crystals %	Crystal size range from (μm)	to (μm)
0.9	118.4	54.9
12.3	54.9	33.7
7.5	33.7	23.7
10.0	23.7	17.7
6.9	17.7	13.6
9.4	13.6	10.5
20.3	10.5	8.1
15.4	8.2	6.4
6.0	6.4	5.0
4.9	5.0	3.9
5.1	3.9	3.0
1.3	3.0	2.4
0.1	2.4	1.9

Run 22 D.

Oilbath temperature : 140 °C

Stirrer speed : 3600 rpm

Drawdown time of vessel : 500. min

Crystal suspension density : 9.25 g/l

Supersaturation Tungstan: 36.29 g/l

Weight fraction of crystals %	Crystal size range from (μm)	to (μm)
1.5	23.7	17.7
8.5	17.7	13.6
13.1	13.6	10.5
15.0	10.5	8.2
22.4	8.2	6.4
31.3	6.4	5.0
8.1	5.0	3.9

Run 23 A.

Oilbath temperature : 140 °C

Stirrer speed : 3600 rpm

Drawdown time of vessel : 368. min

Crystal suspension density : 22.14 g/l

Supersaturation of tungsten: 100.1 g/l

Weight fraction of crystals %	Crystal size range from (μm)	to (μm)
0.1	33.7	23.7
1.2	23.7	17.7
7.9	17.7	13.6
19.5	13.6	10.5
22.8	10.5	8.2
15.5	8.2	6.4
12.9	6.4	5.0
14.2	5.0	3.9
4.8	3.9	3.0
0.7	3.0	2.4
0.2	2.4	1.9

Run 23 B.

Oilbath temperature : 140 °C

Stirrer speed : 3600 rpm

Drawdown time of vessel : 49.4 min

Crystal suspension density : 0.442 g/l

Supersaturation of tungsten: 52.99 g/l

Weight fraction of crystals %	Crystal size range from (μm)	to (μm)
0.1	13.6	10.5
2.0	10.5	8.2
9.3	8.2	6.4
19.1	6.4	5.0
20.7	5.0	3.9
16.6	3.9	3.0
15.0	3.0	2.4
9.5	2.4	1.9
3.4	1.9	1.5
4.3	1.5	1.2

Run 23 C.

Oilbath temperature : 140 °C

Stirrer speed : 3600 rpm

Drawdown time of vessel : 109.5 min

Crystal suspension density : 2.45 g/l

Supersaturation of tungsten: 65.71 g/l

Weight fraction of crystals %	Crystal size range from (μm)	to (μm)
0.4	23.7	17.7
4.0	17.7	13.6
18.0	13.6	10.5
28.2	10.5	8.2
13.7	8.2	6.4
5.4	6.4	5.0
6.5	5.0	3.9
7.7	3.9	3.0
6.1	3.0	2.4
4.3	2.4	1.9
2.2	1.9	1.5
3.4	1.5	1.2

Run 23 D.

Oilbath temperature : 140 °C

Stirrer speed : 3600 rpm

Drawdown time of vessel : 109.5 min

Crystal suspension density : 4.043 g/l

Supersaturation of tungsten: 67.25 g/l

Weight fraction of crystals %	Crystal size range from (μm)	to (μm)
0.2	33.7	23.7
6.0	23.7	17.7
35.5	17.7	13.6
35.0	13.6	10.5
13.9	10.5	8.2
3.3	8.2	6.4
1.9	6.4	5.0
3.4	5.0	3.9
0.3	3.9	3.0
0.0	3.0	2.4
0.1	2.4	1.9
0.3	1.9	1.5

APPENDIX H

Numerical example of the calculation of the crystallization kinetics from an analysis of the crystal size distribution obtained experimentally for a specific run is presented below.

Run 17 will be used to demonstrate the procedure.

1. A representative sample of the crystallizer magma for each run is analyzed to determine the weight fraction of crystals in each size fraction. This was done by MINTEK using a Malvern particle size analyzer and the results shown in Appendix G. For run 17 the results are:

Weight fraction of crystals %	Crystal size range from (μm) to (μm)
0.3	118.4 54.9
1.5	54.9 33.7
3.5	33.7 23.7
11.3	23.7 17.7
21.4	17.7 13.6
22.2	13.6 10.5
20.8	10.5 8.2
8.8	8.2 6.4
4.5	6.4 5.0
5.2	5.0 3.9
0.4	3.9 3.0

2. The characteristic size L for the size range corresponding to each mass fraction in the distribution is determined. This characteristic size is taken as the mid-point of every size range, i.e. for the size range 33.7 μm to 23.7 μm the characteristic size L is (33.7+23.7)/2.

For run 17 the results are:

Weight fraction of crystals %	Characteristic size L (μm)
0.3	86.65
1.5	44.3
3.5	28.7
11.3	20.7
21.4	15.65
22.2	12.05
20.8	9.35
8.8	7.3
4.5	5.7
5.2	4.45
0.4	3.45

3. A suitable shape factor for the crystals is determined. According to figure 6.4 the assumption of spherical crystals is adequate. Using this assumption and the expression for the volume of a spherical crystal, the shape factor can be calculated as follows:

Volume of crystal = $k_v . L^3$ H.1

Where: k_v = Volume shape factor.
L = Characteristic crystal size.

Using equation H.1 and the known expression for the volume of a sphere k_v is calculated:

Volume of sphere = $\pi/6\ L^3 = k_v\ L^3$

It follows from the above expression that k_v is $\pi/6$.

For run 17 the results are:

Weight fraction of crystals %	Characteristic size L (μm)
0.3	86.65
1.5	44.3
3.5	28.7
11.3	20.7
21.4	15.65
22.2	12.05
20.8	9.35
8.8	7.3
4.5	5.7
5.2	4.45
0.4	3.45

3. A [illegible] shape factor for the crystals is determined. According to figure 6.4 the assumption of spherical crystals is adequate. [illegible] this assumption and the expression for the volume of a spherical crystal, the shape factor can be calculated as follows:

Volume of crystal = $k_v . L^3$ H.1

Where: k_v = Volume shape factor.
L = Characteristic crystal size.

Using equation H.1 and the known expression for the volume of a sphere k_v is calculated:

Volume of sphere = $\pi/6\ L^3 = k_v\ L^3$

It follows from the above expression that k_v is $\pi/6$.

4. The results obtained from MINTEK is in mass fractions. The population density n calculated for each size range is based on a unit volume of crystallizer slurry. In order to put the computation on this basis the crystal suspension density must be known and this must be multiplied by the different mass fractions for each size range. The result is the mass of crystals in each size range per unit volume of crystallizer slurry.

With this mass distribution per unit volume of suspension known, the population density of each characteristic size can be determined by the following expression:

$$(n)_L = (M_t \Delta W)/(\rho k_v L^3 \Delta L) \qquad H.2$$

Where: $(n)_L$ = Population density as a funtion of crystal size (number of crystals/ml.μm).
M_t = Crystal suspension density (g/ml).
ΔW = Weight fraction of crystals in the size range L_1 to L_2 (-).
ρ = Absolute density of the crystalline species (g/ml).
k_v = Volume shape factor (-).
L = Characteristic size for the size range L_1 to L_2 (μm).
ΔL = $L_2 - L_1$ (μm).

For run 17: $(n)_L = (40.98 \text{ g/l} * \Delta W)/(5662 \text{ g/l} * \frac{\pi}{6} * L^3 * \Delta L)$

Using the data in the above two tables the resulting population densities for run 17 can be calculated as:

Crystal population density (num/ml.μm)	Characteristic size L (μm)
1.496 E6	3.45
7.414 E6	4.45
2.399 E6	5.7
1.737 E6	7.3
1.529 E6	9.35
5.657 E5	12.05
1.882 E5	15.65
2.933 E4	20.7
2.046 E3	28.7
1.125 E2	44.3
1.004	86.65

5. A plot of ln n versus L is plottad for each run and the crystallization kinetics i.e. nucleation and growth rates calculated using this plot. This procedure will now be illustrated.

The semilog plot of population density versus crystal size for run 17 looks as follows:

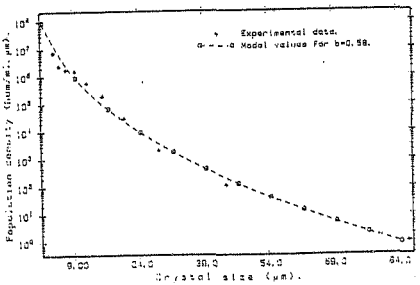

From the above figure it can be seen that the plot is non-linear. Reasons for this behaviour have been presented in section 6.4.3. It was concluded that size dependant growth kinetics dominates the system and a size dependent growth rate model was proposed. This model was fitted to the experimental results of run 17 with the procedure described in section 6.5. The following results were obtained.

Nuclei population density $n^* = 2.5E9$ num/ml.μm

Nuclei-sized crystal growth rate $G^* = 7.00E{-}3$ μm/min

Size dependent crystal growth rate $G = 7.00E{-}3(1+2.116\ L)^{0.58}$ μm/min

According to Abegg, Stevens and Larson (1968) the crystal nucleation rate is the product of the nuclei population density and the nuclei-sized crystal growth rate:

Crystal nucleation rate $B^* = 1.75E7$ num/ml.min

APPENDIX I

Calculated population density distributions for the various runs.

The experimental conditions and raw data for each of these runs are summarised in Appendix J.

The population density distributions were calculated for each run with the method described in Appendix H. A size dependent growth rate model was fitted to these data and from this model the growth and nucleation kinetics of crystallization followed: The nuclei population density n° and nuclei-sized crystal growth rate G° were used as the two parameters to fit the size dependent growth rate model to the data. According to Abegg, Stevens and Larson (1968) the crystal nucleation rate is the product of these two values n° and G°. The size dependent crystal growth rate G is expressed by the growth rate model fitted to the experimental data.

Run 14.

Nuclei population density (n°) : 2.21 E7 number/ml.μm

Nuclei-sized crystal growth rate (G°): 7.36 E-2 μm/min.

Nucleation rate (B°) : 1.63 E6 num/ml.min

Crystal growth rate (G) : $7.36E\text{-}2(1+0.275\ L)^{0.58}$ μm/min

Crystal population density (num/ml.μm)	Characteristic size L (μm)
1.064 E7	1.7
1.683 E7	2.15
1.416 E7	2.7
1.018 E7	3.45
1.251 E7	4.45
5.402 E6	5.7
1.552 E6	7.3
8.561 E5	9.35
7.207 E5	12.05
3.778 E5	15.65
6.638 E4	20.7
5.305 E3	28.7
1.701 E2	44.3

Run 15

Nuclei population density (n^*) : 1.274 E7 number/ml.μm

Nuclei-sized crystal growth rate (G^*): 6.07 E-2 μm/min.

Nucleation rate (B^*) : 7.73 E5 num/ml.min

Crystal growth rate (G) : $6.07E\text{-}2(1+0.339\ L)^{0.58}$ μm/min

Crystal population density (num/ml.μm)	Characteristic size L (μm)
8.494 E6	1.35
6.381 E6	1.7
7.570 E6	2.15
5.309 E6	2.7
5.998 E6	3.45
3.881 E6	4.45
8.464 E5	5.7
4.745 E5	7.3
5.302 E5	9.35
3.063 E5	12.05
9.455 E4	15.65
1.296 E4	20.7
7.426 E2	28.7
3.402	44.3

Run 17.

Nuclei population density (n^*) : 2.5 E9 number/ml.μm

Nuclei-sized crystal growth rate (G^*): 7.00 E-3 μm/min.

Nucleation rate (B^*) : 1.75 E7 num/ml.min

Crystal growth rate (G) : $7.00E\text{-}3(1+2.116\ L)^{0.58}$ μm/min

Crystal population density (num/ml.μm)	Characteristic size L (μm)
1.496 E6	3.45
7.414 E6	4.45
2.399 E6	5.7
1.737 E6	7.3
1.529 E6	9.35
3.657 E5	12.05
1.882 E5	15.65
2.935 E4	20.7
2.046 E3	28.7
1.125 E2	44.3
1.004	86.65

Run 18.

Nuclei population density (n^*) : 9.96 E9 number/ml.μm

Nuclei-sized crystal growth rate (G^*): 4.94 E-3 μm/min.

Nucleation rate (B^*) : 4.92 E7 num/ml.min

Crystal growth rate (G) : $4.94E\text{-}3(1+3.0\ L)^{0.58}$ μm/min

Crystal population density (num/ml.μm)	Characteristic size L (μm)
1.064 E7	1.7
1.683 E7	2.15
1.416 E7	2.7
1.018 E7	3.45
1.251 E7	4.45
5.402 E6	5.7
1.532 E6	7.3
8.561 E5	9.35
7.207 E5	12.05
3.778 E5	15.65
6.638 E4	20.7
5.305 E3	28.7
1.701 E2	44.3

Run 19.

Nuclei population density (n^*) : 7.17 E8 number/ml.μm

Nuclei-sized crystal growth rate (G^*): 1.0 E-2 μm/min.

Nucleation rate (B^*) : 7.17 E6 num/ml.min

Crystal growth rate (G) : $1.0E\text{-}2(1+1.482\ L)^{0.58}$ μm/min

Crystal population density (num/ml.μm)	Characteristic size L (μm)
2.402 E7	1.35
1.804 E7	1.7
2.140 E7	2.15
4.503 E6	2.7
4.797 E5	3.45
1.661 E6	5.15
2.987 E6	7.3
8.486 E4	9.35
1.634 E5	12.05
4.411 E5	15.65
1.106 E5	20.7
3.974 E3	28.7
1.924 E1	44.3

Run 19

Nuclei population density (n^*) : 7.17 E8 number/ml.μm

Nuclei-sized crystal growth rate (G^*): 1.0 E-2 μm/min.

Nucleation rate (B^*) : 7.17 E6 num/ml.min

Crystal growth rate (G) : $1.0E\text{-}2(1+1.482\ L)^{0.58}$ μm/min

Crystal population density (num/ml.μm)	Characteristic size L (μm)
2.402 E7	1.35
1.804 E7	1.7
2.140 E7	2.15
4.503 E6	2.7
4.797 E5	3.45
1.661 E6	5.15
2.987 E6	7.3
8.486 E4	9.35
1.634 E5	12.05
4.411 E5	15.65
1.106 E5	20.7
3.974 E3	28.7
1.924 E1	44.3

Run 20.

Nuclei population density (n^*) : 2.07 E7 number/ml.μm

Nuclei-sized crystal growth rate (G^*): 4.4 E-2 μm/min.

Nucleation rate (B^*) : 9.12 E5 num/ml.min

Crystal growth rate (G) : $4.4E\text{-}2(1+0.446\ L)^{0.58}$ μm/min

Crystal population density (num/ml.μm)	Characteristic size L (μm)
4.155 E6	1.7
7.394 E5	2.15
2.420 E6	2.7
1.878 E6	3.45
2.948 E6	4.45
1.307 E6	5.7
7.754 E5	7.3
5.842 E5	9.35
2.017 E5	12.05
3.039 E4	15.65
1.841 E3	20.7
3.454 E1	28.7

Run 22 A.

Nuclei population density (n^*) : 7.0 E6 number/ml.μm

Nuclei-sized crystal growth rate (G^*): 1.05 E-2 μm/min.

Nucleation rate (B^*) : 7.35 E4 num/ml.min

Crystal growth rate (G) : $1.05E\text{-}2(1+1.211\ L)^{0.58}$ μm/min

Crystal population density (num/ml.μm)	Characteristic size L (μm)
8.296 E4	2.7
1.326 E5	3.45
2.055 E5	4.45
1.713 E5	5.7
6.343 E4	7.3
1.563 E4	9.35
4.697 E3	12.05
1.974 E3	15.65
6.321 E2	20.7
1.409 E2	28.7
2.286 E1	44.3
4.111 E-1	86.65

Run 22 C.

Nuclei population density (n°) : 8.5 E6 number/ml.μm

Nuclei-sized crystal growth rate (G°): 8.00 E-3 μm/min.

Nucleation rate (B°) : 6.8 E4 num/ml.min

Crystal growth rate (G) : $8.00E\text{-}3(1+1.590\ L)^{0.58}$ μm/min

Crystal population density (num/ml.μm)	Characteristic size L (μm)
3.172 E4	2.15
1.735 E5	2.7
2.175 E5	3.45
7.969 E4	4.45
3.648 E4	5.7
3.467 E4	7.3
1.702 E4	9.35
2.732 E3	12.05
6.922 E2	15.65
2.962 E2	20.7
5.001 E1	28.7
1.052 E1	44.3
3.434 E-2	86.65

Run 22 D.

Nuclei population density (n^*) : 3.91 E6 number/ml.μm

Nuclei-sized crystal growth rate (G^*): 3.91 E-3 μm/min.

Nucleation rate (B^*) : 1.53 E5 num/ml.min

Crystal growth rate (G) : $3.91E\text{-}3(1+0.512\ L)^{0.58}$ μm/min

Crystal population density (num/ml.μm)	Characteristic size L (μm)
2.607 E6	4.45
1.766 E6	5.7
9.980 E5	7.3
2.489 E5	9.35
7.535 E4	12.05
1.687 E4	15.65
8.793 E2	20.7

Run 23 A.

Nuclei population density (n^*) : 8.42 E7 number/ml.μm

Nuclei-sized crystal growth rate (G^*): 5.31 E-3 μm/min.

Nucleation rate (B^*) : 4.47 E5 num/ml.min

Crystal growth rate (G) : $5.31E-3(1+0.511\ L)^{0.58}$ μm/min

Crystal population density (num/ml.μm)	Characteristic size L (μm)
3.005 E6	2.15
4.426 E6	2.7
9.699 E6	3.45
1.094 E7	4.45
3.715 E6	5.7
1.664 E6	7.3
9.056 E5	9.35
2.685 E5	12.05
3.754 E4	13.65
1.684 E3	20.7
3.[illegible]9 E1	28.7

Run 23 R.

Nuclei population density (n°) : 3.37 E7 number/ml.μm

Nuclei-sized crystal growth rate (G°): 1.84 E-2 μm/min.

Nucleation rate (B°) : 6.21 E5 num/ml.min

Crystal growth rate (G) : $1.84E\text{-}2(1+1.098\ L)^{0.58}$ μm/min

Crystal population density (num/ml.μm)	Characteristic size L (μm)
2.828 E6	1.35
2.579 E6	1.7
2.650 E6	2.15
1.893 E6	2.7
6.696 E5	3.45
3.184 E5	4.45
1.099 E5	5.7
1.980 E4	7.3
1.586 E3	9.35
2.748 E1	12.05

Run 23 C.

Nuclei population density (n°) : 1.69 E7 number/ml.μm

Nuclei-sized crystal growth rate (G°): 1.55 E-2 μm/min.

Nucleation rate (B°) : 2.62 E5 num/ml.min

Crystal growth rate (G) : $1.55E\text{-}2(1+0.590\ L)^{0.58}$ μm/min

Crystal population density (num/ml.μm)	Characteristic size L (μm)
1.119 E7	1.35
9.251 E6	1.7
7.151 E6	2.15
4.268 E6	2.7
1.722 E6	3.45
5.541 E5	4.45
1.721 E5	5.7
1.617 E5	7.3
1.239 E5	9.35
2.742 E4	12.05
2.103 E3	15.65
6.211 E1	20.7

Run 23 D.

Nuclei population density (n°) : 1.93 E6 number/ml.μm

Nuclei-sized crystal growth rate (G°): 2.86 E-2 μm/min.

Nucleation rate (B°) : 5.51 E4 num/ml.min

Crystal growth rate (G) : $2.86E\text{-}2(1+0.3i9\ L)^{0.58}$ μm/min

Crystal population density (num/ml.μm)	Characteristic size L (μm)
1.847 E6	1.35
2.082 E6	1.7
2.744 E5	2.15
8.725 E4	3.15
4.783 E5	4.45
9.993 E4	5.7
6.426 E4	7.3
1.008 E5	9.35
8.799 E4	12.05
3.080 E4	15.65
1.537 E3	20.7
1.154 E1	28.7

APPENDIX J

Development of the predominant crystal size (Randolph and Larson, 1971).

The fundamental population balance equation has been derived in section 3.2 as follows:

$$n = n^{\circ} \exp\left(\frac{-L}{Gr}\right) \qquad J.1$$

For the fundamental population balance equation the quantity L/Gr is dimensionless. By replacing it with the dimensionless length $x = L/Gr$ the following equation is obtained:

$$n = n^{\circ} \exp^{-x} \qquad J.2$$

The population number, length, area and mass are obtained from normalized moment equations as shown in section 3.2. The third moment equation, normalized, of the crystal population is:

$$\mu_3 = \frac{\int_0^x x^3 e^{-x}\, dx}{\int_0^{\infty} x^3 e^{-x}\, dx} \qquad J.3$$

Equation J.3 is called the normalized mass cumulative fraction.

After the integration of equation J.3:

$$\mu_3 = 1 - (1 + x + 1/2\ x^2 + 1/6\ x^3)\ e^{-x} \qquad J.4$$

Differentiating equation J.4 with respect to x gives the following result:

$$\frac{d\ \mu_3}{dx} = \frac{x^3\ e^{-x}}{6} \qquad J.5$$

A plot of equation J.4 is shown in figure J.1 and for equation J.5 in figure J.2. From figure J.2 it is seen that the predominant crystal size is at a value of x = 3.

Since x=L/Gr the predominant crystal size is where L=3Gr.

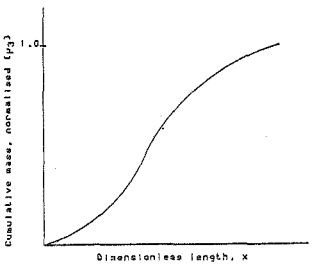

Figure J.1 Plot of the cumulative mass distribution

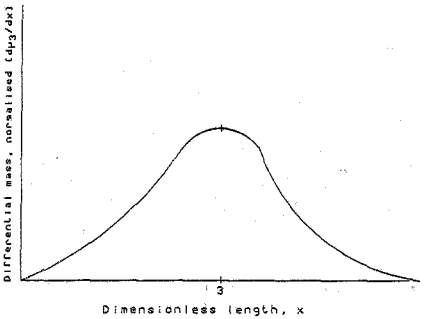

Figure J.2 Plot of the differential mass distri

APPENDIX K

Derivation of the population balance equation if size-dependant growth of the crystals is assumed.

The general population balance equation derived by deriving the population balance over a Macroscopic External Coordinate Region will be used as a starting point to derive the population balance equation if growth rate is size-dependant. This population balance over a Macroscopic External Coordinate Region has been derived by Randolph and Larson (1971). (Refer to section 3.1 for the derivation of the general population balance equation.)

This general population balance can be used for describing transient and steady-state particle-size distributions in well-mixed, continuous, isothermal vessels:

$$\frac{\delta n}{\delta t} + \frac{\delta (Gn)}{\delta L} + D - B + n \frac{d(\log V)}{dt} = -\sum_j \frac{n_j Q_j}{V} \qquad K.1$$

Assuming that all the constraints for an ideal crystallizer, except McCabe's ΔL law, hold the population balance equation for a crystallizing system with size-dependant growth can then be derived.

Because of the constraints of steady state, no crystals in the feed stream, and no birth and death terms equation K.1 reduces to:

$$\frac{d(Gn)}{dL} + \frac{Qn}{V} = 0 \qquad K.2$$

Stating that V/Q=τ and using the size dependant growth rate expression $G=G^*(1+\gamma L)^b$ as described in section 3.4 equation K.2 reduces to:

$$\frac{d[nG^*(1+\gamma L)^b]}{dL} + \frac{n}{\tau} = 0 \qquad \text{K.3}$$

This equation K.3 can be simplified to give the following result:

$$\int_{n^*}^{n} \frac{dn}{n} = -\frac{1}{\tau G^*} \int_{0}^{L} \frac{dL}{(1+\gamma L)^b} - b\gamma \int_{0}^{L} \frac{dL}{(1+\gamma L)} \qquad \text{K.4}$$

and after integration of equation K.4:

$$\ln n = \ln n^* + \frac{1}{1-b} \cdot \frac{(1+\gamma L)^{1-b}}{1-b} - b \ln (1+\gamma L) \qquad \text{K.5}$$

which, if simplified, is the resulting population balance equation for a system with size-dependent crystal growth rates:

$$n = K_3\, n^*(1+\gamma L)^{-b} \exp\left[-\frac{(1+\gamma L)^{1-b}}{1-b}\right] \qquad \text{K.6}$$

Where $K_3 = \exp\left(\frac{1}{1-b}\right)$

$$\gamma = \frac{1}{G^*\tau}$$

$$b < 1$$

For b=0, equation K.6 gives the size distribution corresponding to McCabe's ΔL law.

APPENDIX L

Calculation of the membrane efficiencies for the electrolytic cell operation.

The membrane efficiency of an electrolytic cell has previously been defined in Appendix D as:

$$\eta = \frac{\text{Observed sodium flux}}{\text{Theoretical maximum flux}} * 100\ \% \qquad \text{L.1}$$

The maximum flux is the flux which will be observed if sodium ions are the only ions which move through the membrane. The expression for maximum flux can be derived using Faraday's law as expressed in Appendix G:

$$t = \frac{m\ Z\ F}{M\ I\ \eta} \qquad \text{L.2}$$

Where: t = Time needed (s).
m = Mass of sodium ions to be transported per unit area (g/cm^2).
Z = Number of charges on the sodium ion (-).
F = Faraday's constant (96485 C/mol).
M = Atomic weight of sodium (g/mol).
I = Current density (A/cm^2).
η = Membrane efficiency (-).

The maximum flux will be obtained when the membrane efficiency is 100%. Thus, when η=1. The number of charges on a sodium ion, and therefore Z, is one. Taking this into account, equation L.2 can be rearranged to give an expression for the maximum flux through the membrane:

$$N = \frac{I}{F} \qquad L.3$$

Where: N = Molar flux of the sodium ions ($mol/cm^2.s$).

The actual sodium flux will be given as:

$$N_{actual} = \frac{d(VC)}{dt} \qquad L.4$$

Where : V = Catholyte volume.
C = Sodium concentration in catholyte.

If the volume of the catholyte solution is constant equation L.4 can be reduced to:

$$N_{actual} = \frac{VdC}{dt} \qquad L.5$$

This differential is the slope of the curve obtained when the sodium concentration in the catholyte is plotted against the running time of the cell. It must be noted that, in order to use this equation, the catholyte volume must be constant. This does not happen since samples are taken from the solution to determine the sodium concentration with the result that the volume decreases each time. This problem was overcome by correcting the sodium concentration in the catholyte for the loss in volume by sampling. This meant that all the sodium concentrations were based on the same volume basis, and hence equation L.5 could be used.

A run was done to illustrate this procedure. The experimental data look as follows:

Current density = 1000 A/m^2
Solution temperature = 40 °C
Catholyte volume = 6 l
Anolyte volume = 6.4 l

Time (hr)	Cell voltage	Catholyte Na conc. ($g.l^{-1}$)	Corrected Na conc. ($g.l^{-1}$)
0.0	11.5	0.075	0.075
0.5	11.0	0.897	0.893
1.0	10.5	2.069	2.06
1.5	9.5	2.862	2.84
2.25	8.5	4.552	4.51
3.0	8.5	6.138	6.07
4.0	8.5	8.138	8.03
4.5	9.0	9.172	9.03
5.0	9.2	10.00	9.82
5.5	9.3	11.034	10.81
6.0	9.3	11.897	11.64
6.25	9.4	12.241	11.96
6.5	9.5	12.414	12.11
7.0	9.6	12.758	12.42
7.5	9.7	12.931	12.56
8.0	9.8	13.276	12.88

These data are used to plot the graph of Na concentration in the catholyte versus the running time of the cell as is done in figure 6.1.

From figure 6.1 it follows that the slope of the first part of the curve is 1.96. The volume of the catholyte solution is known as 6l and the area of the electrode plates is 200cm^2. Thus, from equation L.5:

N_{actual} = (1.96 * 6) / (200 * 23)
= 0.0071 mol/s.cm^2

Knowing that the current density in the electrolytic cell is 1000 A/cm^2 the maximum sodium flux can then be calculated using equation L.3:

$$N_{max.} = 1000 / 96485$$
$$= 0.0104 \text{ mol/s.cm}^2$$

The membrane efficiency, η, is then (from equation L.1):

$$\eta = (0.0071 / 0.0104) \times 100$$
$$= 68.6 \%$$

The same procedure can be followed to calculate the membrane efficiency of the second part of the curve. The efficiency in this part of the curve is calculated as 18%.

APPENDIX M

WATFIV computer program for the simulation of the crystal size distribution of the crystals produced in the MSMPR crystallizer. (Refer to chapter 6.5)

M.1 Algorithm

The main program initialises the program, and calls an optimisation routine from the I.M.S.L. library to minimise the sum of squared errors. The optimisation program ZXMIN minimises the sum of squared errors calculated in the subroutine FUNC for the three parameters b, G^* and n^*. The program ZXMIN uses a quasi-Newton method to find the minimum of a function f(x) of N variables.

The subroutine FUNC calculates the sum of squared differences between the measured crystal size distribution data and the simulated crystal size distributions, as calculated using the proposed size dependent crystal growth rate model, for a particular combination of the parameters b, G^* and n^*.

M.2 Program-main

```
$JOB
      EXTERNAL FUNC
      INTEGER M,N,NSIG,MAXFN,IOPT,I,IER
      REAL X(3),FF(20),W(9),H(5),G(3),F,Y(20),NN(20),L(20),T,K1,K2,NO,
      REAL K3,K4,K5,K6,LL(20)
      COMMON /EXDA/Y,L,NN,LL,M,T

C Read in the initial conditions and the measured data.
```

```
      READ (3,*)M,T
      READ (3,*)X(1),X(2),X(3)
      DO 5 I=1,M
      READ(3,*)L(I),Y(I)
    5 CONTINUE

C Secify the convergence criterions, etc. for the I.M.S.L. subroutine
C ZXMIN.

      N=3
      NSIG=12
      MAXFN=5000
      IOPT=3
      CALL ZXMIN(FUNC,N,NSIG,MAXFN,IOPT,X,H,G,F,W,IER)

C Printing the results obtained.

      WRITE (7,1000)X(1),X(2),X(3)
 1000 FORMAT(5X,F5.2,3X,F12.8,3X,F12.8)
      WRITE(7,1001)IER
 1001 FORMAT(5X,I6)
      WRITE(7,1002)F
 1002 FORMAT(5X,F8.4)
      WRITE(7,1003)G(1)
 1003 FORMAT(5X,F8.4)
      WRITE(7,1004)G(2)
 1004 FORMAT(5X,F8.4)
      WRITE(7,1005)W(1)
 1005 FORMAT(5X,F8.4)
      WRITE(7,1006)W(2)
 1006 FORMAT(5X,F8.4)
      WRITE(7,1007)W(3)
 1007 FORMAT(5X,F8.4)
      DO 20 I=1,M
      WRITE(7,101)L(I),Y(I),NN(I)
  101 FORMAT(5X,F6.2,3X,F12.8,3X,F12.8)
   20 CONTINUE
      STOP
```

```
      END

C Subroutine to calculate the sum of squares.

      SUBROUTINE FUNC(N,X,F)
      INTEGER M,N,I
      REAL X(N),F,Y(20),L(20),K1,K2,K3,K4,K5,K6,NN(20),T,LL(20),FF(20)
      REAL YY(20)
      COMMON /EXDA/Y,L,NN,LL,M,T
      K1=EXP(1.0/(1.0-X(1)))
      K2=-1.0*X(1)
      F=0.0
      DO 15 I=1,M
      LL(I)=ABS(L(I)/(X(2)*T))
      YY(I)=ABS(Y(I)/X(3))
      K3=LL(I)
      K4=(1.0+K3)**K2
      K5=(1.0+K3)**(1.0-X(1))
      K6=1.0-X(1)
      FF(I)=(ALOG(YY(I))-ALOG((K1*K4*EXP(-1.0*K5/K6))))**2
      F=F+FF(I)
      NN(I)=K1*K4*EXP(-1.0*K5/K6)
   15 CONTINUE
      RETURN
      END
$ENTRY
$STOP
```

APPENDIX N

Raw data for two identical runs, one with initial seed crystals added to the system and one with no seed crystals.

Run 22.A.

Seed crystals has been added to this run.

Oilbath temperature : 140 °C

Stirrer speed : 2400 rpm

Drawdown time of vessel : 78.6 min

Crystal suspension density : 0.968 g/l

Supersaturation of tungsten: 15.05 g/l

Weight fraction of crystals %	Crystal size range from (μm)	to (μm)
5.2	118.4	54.9
12.9	54.9	33.7
10.2	33.7	23.7
10.3	23.7	17.7
9.5	17.7	13.6
7.8	13.6	10.5
9.0	10.5	8.2
13.6	8.2	6.4
13.6	6.4	5.0
6.1	5.0	3.9
1.5	3.9	3.0
0.3	3.0	2.4

Run 22 B.

No seed crystals were added to this run and no tungstic acid crystals were found.

Oilbath temperature : 140 °C

Stirrer speed : 2400 rpm

Drawdown time of vessel : 78.6 min

Crystal suspension density : 0.0 g/l

Supersaturation of tungsten: 15.05 g/l

Samples were taken from this experiment and analysed on the same particle analyser as Run 22 A. The results indicated that no crystals were present in the system.